Development of Atomistic Kerogen Models and Their Applications for Gas Adsorption and Diffusion: A Mini-Review

Amaël Obliger, Colin Bousige, Benoit Coasne, Jean-Marc Leyssale

Development of Atomistic Kerogen Models and their Applications for Gas Adsorption and Diffusion: A Mini-Review

Amaël Obliger,[†] Colin Bousige,[‡] Benoit Coasne,[¶] and Jean-Marc Leyssale[*,†]

[†]*Univ. Bordeaux, CNRS, Bordeaux INP, ISM, UMR 5255, F-33400 Talence, France*

[‡]*Laboratoire des Multimatériaux et Interfaces, UMR CNRS 5615, Univ. Lyon, Université Claude Bernard Lyon 1, F-69622 Villeurbanne, France*

[¶]*Univ. Grenoble Alpes, CNRS, LIPhy, 38000 Grenoble, France*

E-mail: jean-marc.leyssale@u-bordeaux.fr

Abstract

With the emergence of shale gas, numerous atomic-scale models of kerogen have been proposed in the literature. These models, which attempt to capture the structure, chemistry and porosity of kerogens of various types and maturities, are nowadays commonly – if not routinely – used to gain nanoscale insights into the thermodynamics and dynamics of complex and important processes such as hydrocarbon recovery and carbon sequestration. However, modeling such a complex, disordered, and heterogeneous material is a particularly challenging task. It implies that important underlying assumptions and simplifications, which can significantly affect the predicted properties, have to be made when constructing the kerogen models. In this mini review, we discuss the existing atomistic models of kerogen by categorizing them according to the different approaches and assumptions used during their construction. For each type of models, we also describe how the construction strategy can impact the prediction

of certain properties. Important work on kerogen interactions with gas and oil, from both the point of view of equilibrium adsorption (including adsorption-induced deformation) and transport, are described. Possible improvements and upscaling strategies – to better account for kerogen in its geological environment – are also discussed.

1 Introduction

Kerogen, literally "wax producer", is a term that was first used in 1912 by the Scottish organic chemist Alexander Crum Brown, defining sedimentary Organic Matter (OM) that produces oil upon heating.[1] As pointed out by Cane,[2] kerogen's definition has evolved over the years and, nowadays, the term kerogen applies to sedimentary OM that is insoluble in the usual organic solvents. Kerogen is by far the most abundant form of OM on Earth.[3] Its total mass, estimated to $\sim 10^{16}$ tons, is about three orders of magnitude larger than coal and petroleum in conventional reservoirs,[4] and four orders of magnitude larger than the living biomass.[5] Yet, at least until recently, the structure and properties of kerogen have received much less interest than almost any other form of OM, natural or synthetic.[6]

In the course of the 20$^{\text{th}}$ century, scientists and engineers have developed standardized techniques to characterize kerogen. The concept of maturity, which can be measured via quantities like the vitrinite reflectance, defines whether the kerogen is in a state of oil generation (immature), gas generation (mature) or above its hydrocarbon production stage (overmature). Later on, a method inherited from coal science[7] was also applied to kerogen evolution. In this so-called van Krevelen diagram, the evolution (or maturation) of kerogen is characterized through a two-dimensional diagram showing the evolution of the atomic H/C and O/C ratios.[5] It allows identifying three important kerogen families, which can also be classified according to the origin of the OM: type I kerogen, with largest H/C and lowest O/C, originates from lacustrine environments, type II kerogen from marine deposits and type III kerogen, with lowest H/C and largest O/C, from terrestrial plants and animal remains.[3] Type IV kerogen is also sometimes considered to describe kerogen or humic coals with ultra-

low H/C and which can only produce dry gas.[3] This less-common type will be ignored in the remaining of this review. An example of kerogen van Krevelen diagram, showing data of actual kerogen samples and atomistic kerogen models, is shown in Fig. 1. In this diagram, maturity increases from top-right to bottom-left or, in other words, from hydrogen and oxygen rich OM to almost entirely pure carbon. Unlike minerals, whose crystal structure can be straightforwardly and unambiguously determined from experiments (e.g. X-ray diffraction), kerogen is a disordered material with no clearly defined structure– even though some local aromatic order and domain orientation can develop. Nevertheless, the structure evolution during maturation is usually considered as a transition from a cross-linked, mostly aliphatic skeleton, to a disordered, almost entirely aromatic, carbon.[8] A few review articles on kerogen properties were written by Rullkötter and Michaelis,[9] Vandenbroucke,[10] and Vandenbroucke and Largeau,[3] slightly before the advent of unconventional fossil fuels about a decade ago. Then, hydraulic fracking has significantly changed the game in both the energy market and research,[11–13] boosting the number of studies on kerogen.

In the so-called organic-rich shales, that can produce oil and gas, the organic content, up to a maximum of 10% of the source rock in volume,[19] is mostly composed of kerogen in addition to lighter species like asphaltenes and resins, and, of course hydrocrabons and other gases.[20] Therefore, an important effort has been devoted to the establishment of a rigorous description of the intimate relationship between the structure of the host kerogen and the amount and composition of the gas trapped in its porosity, which both contains micropores (< 2 nm) and mesopores (2-50 nm). Considering the intrinsic complexity of the experimental materials, which display a multiscale nature and heterogeneous features both in terms of chemistry and structure, the experimental investigation of the link between kerogen properties and the hydrocarbon phase produced along its evolution is a very challenging task. Despite recent progress in characterization techniques, concerns can be raised regarding the sample preparation, especially the step at which kerogen is isolated from shale's mineral content,[21] and experimental conditions considered when assessing experimentally

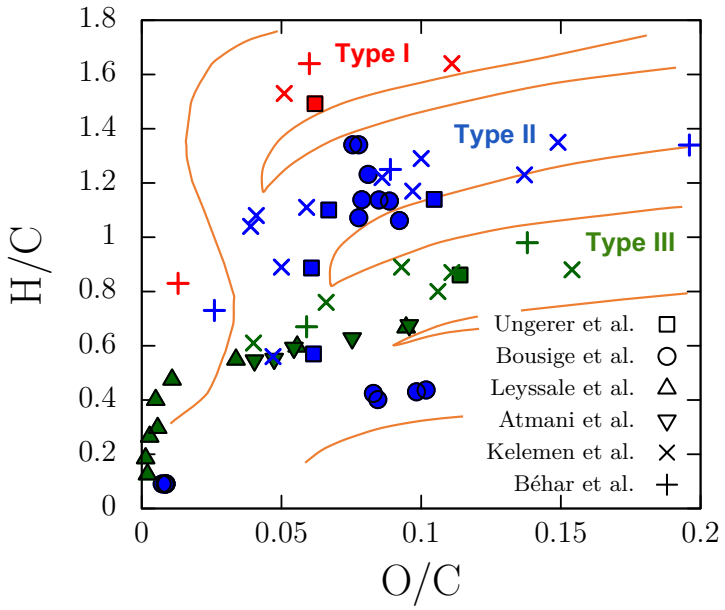

Figure 1: Evolution pathway of the three main kerogen types represented on a Van Krevelen diagram. The molecular models of Ungerer et al. (squares),[14] the reconstructed models of Bousige et al. (circles)[15] and the mimetic models of Atmani et al. and Leyssale et al. (triangles)[16,17] are represented together with experimental data from Kelemen et al.[18] (crosses) and Béhar et al.[8] (pluses). Color code: red (type I), blue (type II) and green (type III).

the gas trapped in the porosity and the dynamical parameters driving its expulsion. Sample treatment and storage conditions that drastically differ from those relevant to kerogen in shale reservoirs may lead to approximate or misleading conclusions.

Molecular simulation techniques are excellent tools to investigate physico-chemical processes at the nanoscale. In recent years, these techniques have been used quite intensively to rationalize and predict the amount, nature and transport properties of the fluid phase in kerogen's porosity. Obviously, the starting point of such simulation strategies is the availability of some atomic-scale representations (or models) of the kerogen itself. In section 2, we review the main strategies for atomistic kerogen model construction. More specifically, we differentiate two important categories of models, although some sub-categories are also discussed. In the first category, directly adapted from coal science,[22,23] we refer to "interpretative" models which are kerogen macromolecules constructed as a way to interpret experimental data. In the second category, referred to as "statistical mechanics based", models are generated ab initio from either a purely disordered state (liquid) or some form of ordered matter (a kerogen precursor), via the use of statistical mechanics techniques. Such methods include molecular dynamics (MD) and/or Monte Carlo (MC) simulations coupled to reactive force fields, allowing to describe chemical bond formation and breaking. These simulation techniques are often adapted from earlier studies on the structural modeling of synthetic porous carbons.[24–26]

Section 3 is devoted to recent molecular simulations in which atomistic kerogen models are used to investigate properties relevant to shale gas/oil recovery and/or carbon dioxide sequestration. Even if the models are necessarily simplified, they can be used to establish relevant structure/property relationships that accurately extrapolate to real materials. In section 3.1, we review available work in the literature discussing the connection between the kerogen structural and chemical properties and the gas content and composition in its porosity. We also cover contributions that considered the impact of the pore network morphology and topology (e.g. kerogen's multiporosity, pore shape and accessibility). As part of this

section devoted to the thermodynamics of shale gas in kerogen, we also consider the effect of moisture content and CO_2 injection as this is relevant to important practical aspects: hydraulic fracturing, enhanced oil/gas recovery, and carbon dioxide sequestration. Finally, while this has received less attention in the literature, we also discuss poromechanics of shale gas in kerogen as the rather compliant nature of kerogen is known to lead to important adsorption/desorption-induced deformation of this host material.

Investigating transport properties of the OM is crucial to assess the productivity of hydrocarbon recovery or carbon sequestration processes. However, the complexity and the multiscale nature of source rocks reservoirs makes it difficult to study hydrocarbon transport that remains not fully understood.[27] If different large scale phenomena can affect the fluid flow within such reservoirs ,[28–34] the kerogen microporosity is thought to control the transport properties.[35] In section 3.2, we cover the recent literature on kerogen transport properties, obtained from MD simulations and making use of atomistic kerogen models. Then, in section 3.3, we consider multiscale studies accounting for the impact of mesopores while integrating the transport and adsorption properties determined from kerogen models.

The application of molecular simulations in the context of oil shale kerogen has been the subject of another recent review article,[36] sharing many citations with the present one. However, while assumptions and simplifications are often made in modeling kerogen structure and properties, rather based on practical and technical issues than on physical relevance, their impact on predicted properties is generally not discussed. The originality of this mini-review is that we focus on the various categories of kerogen models, highlighting the consequences of the construction strategies and of the adopted simulation setups on the predicted properties, in addition to other effects like maturity, density, moisture, etc. Also, in line with the general scope of this review, we only consider atomistic kerogen models that account for the complex, disordered nature of this material. Therefore, investigations in which kerogen porosity is considered using simple geometry – such as slit pores – are neglected. For instance, some studies[37,38] can be found about confinement effect on transport in organic

nanopore using molecules of kerogens only to mimic the surface roughness of idealized slit pores without considering the amorphous nature of the kerogen itself, and fluid adsorption within micropores. However, dual porosity investigations in which mesopores are included, even under simple geometries such as slit pores, within a microporous continuum (i.e. a disordered, microporous kerogen model) are considered (e.g. refs. [37–39]). Moreover, considering that a review paper in the same issue is dedicated to Machine Learning approaches, we only consider papers dealing with such techniques when the focus is on the kerogen model (e.g. ref. [40]) and omit other contributions even if we are aware of examples applied to methane adsorption in kerogen models.[41] Also, despite sharing many similarities with kerogen, the large body of literature regarding coal models is mostly ignored. Only considered are coal-focused papers having direct impact, including methodological impact, on kerogen studies. Finally, to conclude this review, we provide in section 4 a discussion on possible future research directions that would allow building more realistic kerogen models, together with better treatment of fluid adsorption and transport, and, eventually, better models of the hydrocarbon recovery process and the carbon sequestration process.

2 Kerogen Models

2.1 Interpretative models

2.1.1 Early "hand drawn" models

Following earlier works,[42] the first "realistic" chemical models of kerogen were proposed by Béhar and Vandenbroucke in 1987.[8] These authors drew a series of macromolecules representative of the three main types of kerogen at three important stages in natural evolution: early diagenesis, early catagenesis, and end of catagenesis. Models were constructed by hand, trying to comply as much as possible with various experimental observables: elemental composition, ratios of aromatic, paraffinic and naphtenic carbons, size of aromatic domains,

and distribution of functional groups. In this work, the immature (early diagenesis) models were arbitrarily set to contain about 1500 C atoms, which is impressive for "hand drawn" molecules, giving molecular weights in the 20–30×10^3 Da range. The models at higher maturities were then constructed to respect the weight losses observed during thermogravimetric analysis, up to 79 % for type I kerogen.

Here, it is important to comment on the adopted size for the models. The size for the most immature models was chosen according to the following constraints: (i) satisfy the kerogen property of not being soluble in common organic solvents, the insolubility limit being in the 5–10×10^3 Da range,[3] (ii) not being too large ($\sim$ 3000 atoms) for obvious practical reasons, and (iii) being large enough to capture the statistical representation of the different biomarkers, chemical functionality and aromatic domain orientations within the models. According to the authors themselves, (immature) kerogen is made by an ensemble of macromolecules forming a continuum of molecular masses. Furthermore, upon evolution, kerogen releases lighter molecules (light gases and petroleum) and condenses to form a carbon-rich solid. As mentioned by Béhar and Vandenbroucke,[8] at some evolution stage, "*it is no longer possible to discuss the structure of kerogen in terms of size, as long distance orientation, similar to that in crystals or polymers, appears*". The decreasing molecular weight with increasing maturity, which was adopted in Béhar and Vandenbroucke's work for practical reasons (i.e. highlighting the mass loss during evolution), was thus somehow unfortunate and misleading as it does not consider the reticulation (cross-linking) of the kerogen during maturation.

A few years after this seminal work, some similar molecular models were proposed by Siskin et al. for the Rundle Ramsay Crossing and Green River type I oil shales.[43] The produced models were made of few independent molecules, some well below the insolubility limit, and should rather be considered as models of the OM than the kerogen stricto sensu. Although these models are strictly 2D, with no attempt to capture the orientation of aromatic fragments, they incorporate the olefinic carbon content, which was not the case in ref. [8]. A unimolecular model of Estonian kukersite kerogen was proposed by Lille et al.[44] and

validated with respect to empirical (i.e. non ab initio) Nuclear Magnetic Resonance (NMR) calculations.

2.1.2 3D Molecular Models

Closely following Béhar and Vandenbroucke's work, Faulon et al.[45] proposed in 1990 an automated computer-aided procedure to build representative kerogen macromolecules in 3D from the same set of data. This procedure, based on creating bonded networks from a distribution of molecular fragments, was applied to a type III kerogen at the end of catagenesis. This model, although made of a single molecule, showed that microporosity occurs naturally in mature type III kerogen due to bond distance and angle constraints.

In 2009, Zhang et al.[46] built a 3D molecular model of Green River kerogen, by slightly modifying Béhar and Vandenbroucke's type I kerogen molecule, and investigated some thermodynamic properties of the material – glass transition temperature, density, thermal expansion coefficients, and solubility parameter – using molecular dynamics (MD) simulations. To our knowledge, it constitutes the first investigation of kerogen using MD. A few years later, Orendt et al.[47] created a digitized version of Siskin's Green River kerogen molecular model using a combination of MD and ab initio calculations. They compared the computed ^{13}C NMR chemical shifts and pair distribution functions to experimental NMR and X-ray diffraction results, showing reasonable agreement.

In 2012, Ru et al.[48] proposed a model of Chinese Huadian oil shale kerogen (type I, immature). A rather small (680 atoms) kerogen "molecule" was generated using a molecular builder by imposing, as done in Béhar and Vandenbroucke,[8] a set of chemical and structural parameters derived from elemental analysis, NMR and XPS data. The model was then relaxed in 3D using molecular mechanics and investigated using MD.

In 2015 and with a similar approach to the one of Ru et al.,[48] Ungerer et al. constructed six molecular models of kerogen, including an immature type I kerogen, an immature type III kerogen, and type II kerogens at four different maturities.[14] The molecules were generated

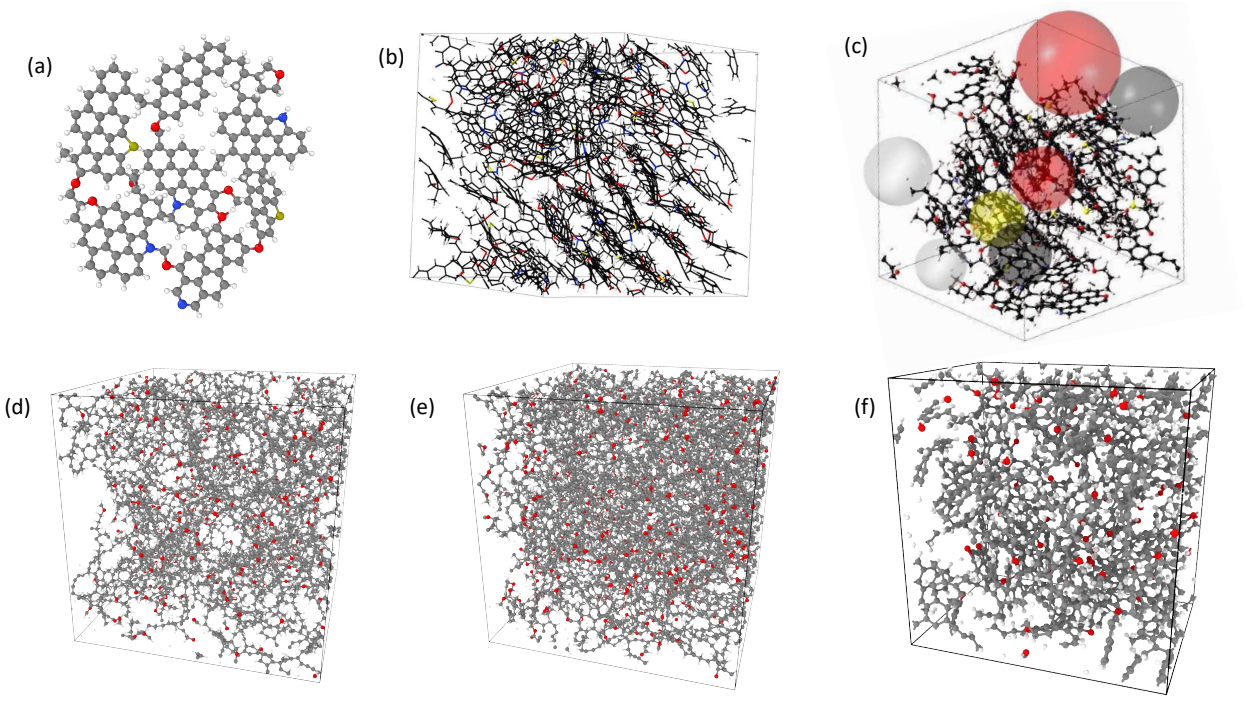

Figure 2: (a) Molecular model of mature (type II-D) kerogen containing C, H, O, N and S atoms.[14] When packed and relaxed in a simulation box (b), such models give rise to ultra-micro porosity[49,50] (Reproduced with permission from ref 14. Copyright 2014 American Chemical Society). (c) Molecular model of type II kerogen in the middle of the oil window (type II-C) showing larger porosity (represented with colored spheres) obtained by adding explicit fluid molecules and asphaltenes (not shown) during the 3D construction (reproduced with permission from ref 51. Copyright 2014 American Chemical Society). The bottom row shows kerogen models developed using the HRMC method for immature Eagle Ford kerogen samples containing C, H and O atoms, with a porosity of (d) 0.8 g/cm^3 or (e) 1.2 g/cm^3.[15] The porosity of the models is directly linked to the imposed density. (f) Type III kerogen model developed by simulating the geological evolution of lignin with REMD.[16] Unlike the molecular models, HRMC and REMD kerogen models are made of a unique cross-linked carbon skeleton percolating through the periodic boudaries of the simulation cells.

according to the data available in Kelemen et al.[18] A snapshot of a mature type II kerogen molecule is shown in Fig. 2a. The authors then proposed a strategy to build bulk kerogen models by packing a number of kerogen molecules in a periodic simulation cell using annealing and cooling MD simulations as shown in Fig. 2b. Some properties, including density, heat capacity, and pair distribution functions were computed. However, because of the small size of the constituting molecules and low degree of cross-linking, these models only show an ultra-microporosity (pore diameters < 7 Å).[49,50,52] Extending the porosity range requires dedicated procedures at the bulk model generation stage like inserting explicit fluid molecules[14] (Fig. 2c) or dummy particles of various sizes.[49,50,52] Ungerer's kerogen molecules have been used in numerous simulation studies in the last decade (see the following sections on gas thermodynamics and transport) and are by far the most widely used atomistic kerogen models.

Ungerer's methodology for building "kerogen molecules" was applied to many other kerogen samples, including Chinese Silurian,[53] Huadian[54,55] and Longkou,[56] as well as the US Marcellus shale.[57] In this approach, models are constructed using data from a wide range of experimental techniques, including ultimate (i.e. elemental) analysis, ^{13}C solid state NMR, Fourier Transformed Infra Red spectroscopy (FTIR), X-ray Photoelectron Spectroscopy (XPS), X-ray Diffraction (XRD), etc. In some of these studies, several isomers of the kerogen model are considered, differing in their degree of branching or functional groups localization. The isomer with lowest energy being selected as the more representative.[54–56] Validation of the selected model using ^{13}C NMR chemical shifts computed using density functional theory was also performed in Guan et al.[54] Liu et al. used an iterative refinement strategy, based on empirical NMR calculations, to select the most representative molecule for a Marcellus kerogen sample.[57] A bulk model was then produced and the computed pair distribution function $G(r)$ and structure factor $S(Q)$ were compared to experimental results from X-ray total scattering measurements, showing relatively poor agreement. A similar iterative procedure was also used by Zhang et al. to produce models of five different mature kerogen samples.[58]

A recent refinement in these strategies for constructing kerogen molecules was proposed in the work of Kang et al.,[40] who used a machine learning algorithm with multi-NMR training.[40] Although very promising, the presented molecules could not exceed 600 Da in mass, which is too small to be representative.

2.1.3 Image-guided models

A last worth mentioning interpretative model – that actually sits at the boundary between interpretative and reconstructed (see below) models – is the mature Longmaxi kerogen (type I-II) model constructed by Wang et al. using an Image Guided (IG) approach.[59] In this work, a 3D fully cross-linked and periodic kerogen model is constructed by assembling aromatic fragments – including curved aromatics – and stacks of aromatic fragments with aliphatic cross-links and pores, by combining information from High Resolution Transmission Electron Microscopy (HRTEM) imaging, NMR, and CO_2 adsorption data.

2.2 Statistical mechanics based models

2.2.1 Liquid quench models

Liquid quench molecular dynamics is often used to generate models of amorphous or glassy carbons.[60] In this method, a liquid at a given density is first equilibrated at high temperature using Reactive MD (RMD) and then cooled down to low temperature. Such Quenched Molecular Dynamics (QMD) method was applied by Obliger et al.[61] who built models of immature (H/C = 1.1) and overmature (H/C = 0.1) type I kerogen by varying the quench rate and the hydrogen content in the liquid. Note that O, N and S were not considered in this work.

2.2.2 Reconstruction Models

Contrary to molecular models that focus on reproducing the distribution of chemical functions of the selected samples, reconstruction models rather focus on reproducing their main

physical characteristics. This is done during the reconstruction process through the implementation of constraints prescribed from experimental measurements of, e.g. diffraction data (structure factor or pair distribution function), pore size distribution, etc. The methodology behind these models is based on the Reverse Monte Carlo (RMC) procedure as introduced by McGreevy and Pusztai[62,63] to describe the structure of systems dominated by 2-body interactions. It was later improved to account for more constraints (CRMC) and allow producing fully linked 3D skeletons of porous structures,[25,64–67] to finally reach the Hybrid RMC (HRMC) procedure[24] where the total potential energy is added to the minimization process. In practice, a fixed number of atoms is placed in a simulation box – with periodic boundaries conditions – according to the desired density, and these atoms are then displaced randomly following a Monte Carlo algorithm with Markov chain sampling. The procedure seeks to minimize the error function $\chi^2 = \sum_{i=1}^{N_{bins}} \left(G_{exp}(r_i) - G_{comp}(r_i)\right)^2 / \sigma^2_{exp}(r_i) + E_{pot}/k_B T$, i.e. the comparison between experimental and computed structure factor $S(q)$ or its Fourier transform, the radial pair correlation function $G(r)$, in addition to a potential energy term. In this approach, to apply such a hybrid energy/structure acceptance criterion, the simulated $G_{comp}(r)$ is determined after each atomic displacement and the potential energy is computed with a reactive force field.

Later, it was proposed to use a weight parameter for the energy term[68,69] and optimize it,[70] as well as to perform a simulated quench starting from high temperatures. Compared to the CRMC procedure, HRMC showed that it could reach structures that are more stable and contain a significantly lower proportion of (unphysical) 3-membered rings in carbon cokes[68,69] and bituminous coals.[26] Such reconstructed porous carbons have been used to simulate mature kerogens and their interface with silicates,[71] together with fracture properties of such systems. However, the HRMC method remains computationally expensive for systems containing a few thousand atoms and, to decrease computational time while increasing the ensemble of explored structures, a modified version of HRMC using a simulated quench mixing MD and HRMC[70] was later proposed. This method was then applied to obtain large

structural type II kerogen models of various maturities[15] (a 5 nm side cube containing up to $\sim$ 15k atoms, Fig. 2d-e). In these kerogen models, the only constraints are the density, the C, H and O relative concentrations, and the experimental $G(r)$. This MD-HRMC procedure allowed producing 3D kerogen models that could reproduce the experimental bulk modulus and vibrational density of states, as well as pore size distribution (microporosity probed by CO_2 adsorption) and heats of formation. They were moreover used to simulate fracture properties, with a clear difference between immature (ductile) and mature (fragile) samples.

2.2.3 Mimetic Models (REMD)

Mimetic modeling refers to a class of methods in which structural models of materials are produced by simulating their formation or synthesis, using for instance RMD. Owing to the timescale of natural evolution (i.e. millions of years), the direct use of RMD in which accessible timescales are of $\sim 10^{-8}$ s is prohibited. Therefore, many authors have performed simulations at elevated temperature to compensate for this limitation in timescale, usually using ReaxFF force fields.[72] Noteworthy investigations are those of Salmon et al.[73] on the pyrolysis of an alganean biopolymer, Liu et al.[74] and Qian et al.[75] on the pyrolysis of the Siskin's Green-River oil shale model, and Pawar et al.[76] on the pyrolysis of Ungerer's kerogen models. However, because of the large heating rates ($\geq$ 10 K/ps) and high temperature conditions (typically $\geq$ 2000 K) required to activate chemistry at the picosecond (ps) timescale, these studies mostly showed the liquefaction or gasification of the macromolecules, and not their expected cross-linking and carbonization. Pyrolysis simulation on lignin and cellulose were also reported with similar conclusions.[77,78]

To bypass this timescale limitation, without biasing thermodynamics, Atmani et al.[79] proposed in 2017 to couple RMD with the Replica Exchange MD (REMD) method, initially developed to accelerate the convergence of protein folding simulations taking place over micro to millisecond timescales.[80,81] In REMD, several "replicas" of the same system are simulated in parallel using RMD at a series of temperatures. The lowest temperature

generally corresponds to the temperature of interest, while the largest one is sufficiently high for chemical reactivity to be fast with respect to the simulation time. At regular intervals during the simulation, attempts to swap the atomic configurations of replicas having nearby temperatures are attempted and accepted according to the following modified Metropolis acceptance criterion:

$$A_{ij} = \min\left\{1, \exp\left[\left(\frac{1}{k_B T_i} - \frac{1}{k_B T_j}\right)(\mathcal{U}_i - \mathcal{U}_j)\right]\right\} \tag{1}$$

where the indices i and j label two adjacent replicas (i.e., $j = i \pm 1$), with T_i and T_j their temperatures, and $\mathcal{U}_i$ and $\mathcal{U}_j$ their potential energies. Provided that a sufficient number of replicas are used, ensuring a good overlap in the potential energy distributions between replicas i and j, every replica will be driven towards its own canonical equilibrium distribution.[82] Convergence of the low temperature replicas, benefiting from chemical reactions achieved at elevated temperatures, is thus accelerated by orders of magnitude. Using this method and RMD simulations based on ReaxFF, Atmani et al. have simulated the conversion into kerogen of cellulose[79] and lignin,[16] two constituents of higher plants as prototypes of type III OM. In those simulations, type III kerogen was simulated up to advanced post-mature states, actually up to H/C $\sim$ 0.1 for the lignin precursor.[17] A REMD (lignin) kerogen model at H/C $\sim$ 0.6 is shown in Fig. 2f. Unlike any other models, the kerogen composition along evolution is a pure outcome of the simulations and, as shown in Fig. 1, it is found almost perfectly within the bounds of type III kerogen. Other outcomes of the REMD simulations are, (i) mass loss, to values of $\sim$ 75 and 40 % for cellulose and lignin, respectively, in good agreement with experimental pyrolysis data, and (ii) fluid production (dominated by water in mass). Fluid production is also intimately correlated with the development of large micropores in the kerogen, which can be moderated by fluid expulsion at an early evolution (immature) stage, before the formation of a stiff (aromatic) carbon backbone. Unlike the molecular models, and as obtained for the HRMC models, REMD kerogen models quickly

form a unimolecular structure percolating through the periodic boundary conditions of the simulation cells, at least for the considered system sizes of few nm widths.

2.3 Critical comparison

To compare the models discussed above, we have gathered in Table 1 some important features of the different approaches used to build kerogen models. In particular, it highlights some very different philosophies in the interpretative and statistical-mechanics based models by considering the different inputs and outcomes (or outputs) in the construction strategies.

Table 1: Summary of the different categories and types of kerogen models showing their different inputs (I), outcomes (O) and the computational costs of the 3D model generation. Displayed model types are the molecular (MOL), image-guided (IG), quench molecular dynamics (QMD), hybrid reverse Monter Carlo (HRMC) and replica-exchange molecular dynamics (REMD).

Model category	**Interpretative**		**Statistical mechanics based**		
Model type	**MOL**	**IG**	**QMD**	**HRMC**	**REMD**
Elemental composition	I	I	I	I	O
Functional groups	I	I	-	O	O
Size and connectivity of the structural elements	I	I	O	O	O
Density	O/I[a]	O/I[a]	I	I	O
Porosity	O/I[a]	O/I[a]	O	O	O
Fluid production	-	-	-	-	O
Mechanical properties	O	O	O	O	O
Cost (CPU hours)	10^{3-4} [b]	negligible	10^{3-4}	10^{4}	10^{6-7}

[a] Porosity and density are often artificially imposed by using a simulated fluid or dummy particles during the bulk kerogen generation. [b] Computational cost is due to the MD simulation required to form bulk kerogen.

2.3.1 Chemical accuracy

The chemical accuracy of interpretative models (both molecular and image-guided) is excellent by construction, since both their elemental composition and chemistry (in the sense of the nature and amounts of functional groups) are imposed based upon chemical characterization (NMR, XPS, FTIR, etc.). Nevertheless, it is also worth mentioning that some

arbitrary choices still have to be made in the interpretation of those data, due to insufficient experimental information. For instance, the olefinic content is generally not considered during NMR spectra fitting, and all the corresponding C atoms are considered as part of aromatic rings in Ungerer's models.[14] Similarly, the distinction between aliphatic and naphtenic carbon (-CH_2- groups) is also arbitrary. Among other common simplification in the interpretative models, is the neglect of heptagonal rings from aromatic or naphtenic groups while pentagonal rings are only considered when suiting desired functional groups like pyrrole or thiophene. This ignores both theoretical[83,84] and experimental[85] works showing that pentagons and heptagons represent an important fraction of the total ring content in disordered carbons.

With statistical mechanics-based methods, the elemental composition may either be imposed (QMD, HRMC) or an outcome of the simulations (REMD). In any case, the final distribution of chemical functions within these models is always an outcome of the simulations. However, while these methods are able to reproduce most general characteristics of kerogens – especially the increasing degree of aromaticity and cross-linking with increasing maturity – they still produce models that contain some unrealistic chemical features. The most problematic is probably the abundance of radical sites and poor diversity of O-containing groups. Large amounts of sp hybridized carbons (cumulenes) and few three-member carbon rings were also observed in the HRMC models. This problem is partly due to the limitations of the reactive potentials used in these procedures, and partly due to an insufficient sampling time, preventing the full convergence of the structures. An advantage of statistical-mechanics based methods, however, is that structural disorder, e.g. naphtenic and olefinic carbon atoms as well as non-hexagonal carbon rings, is naturally included in the models. Due to the limitation of the reactive potentials, the statistical-mechanics based models proposed so far only contain C, H and O atoms (only C and H for the QMD models), while kerogen is known to contain significant amounts of N or S atoms, even though in lower amounts than the above mentioned atoms. While this is an evident flaw, one should note that it should play a minor

effect in the simulation of gas adsorption and/or transport within these models, as the latter are largely dominated by the effects of pore size, texture (ring/chain ratio) and the O/C ratio.

2.3.2 Structure and texture

All the kerogen models present some aliphatic and aromatic moieties, of which both size and amounts vary with maturity. What really differentiates between the interpretative and statistical-mechanics based models is that in the former, these properties are constrained, while they are simulation outputs in the latter. Another constraint in the molecular models is the size of the representative molecules. Indeed, it has to be born in mind that, for instance, the six kerogen molecules proposed by Ungerer et al.[14] only contain a maximum of 252 C atoms (i.e. about six time less than the "hand drown" models of Béhar and Vandenbroucke). This corresponds to molecular weight between 2400–3900 Da, i.e. below the insolubility limit, hence quite not complying with the definition of kerogen (insoluble form of OM). Molecular models proposed by other groups are also based on molecules of similar size and, obviously, cannot capture the expected broad mass distribution of actual kerogen, with a lower end sitting at $\sim$ 5–10 $\times$ 10^3 Da. Regarding this point, the IG approach of Wang et al.[59] is a clear improvement, as cross-links are explicitly incorporated in the models. However, some textural elements derived from HRTEM image analysis may be flawed by image artifacts like fringe superimposition or Moiré patterns. Thus, the distribution of 002 fringe lengths, used to determine the size of aromatics in IG models, may give average domain sizes that are significantly smaller than accurate estimations based on X-ray diffraction or Raman spectroscopy,[83,86] even though some authors also found excellent correlations between XRD and HRTEM data for some char samples.[87]

Conversely to the interpretative models, the structure and texture of the kerogen models are direct outcomes of the statistical mechanics based methods. The QMD and HRMC studies have shown that low O-content kerogens (i.e. type I and II) are made from an uni-

molecular structure percolating through the periodic boundary conditions of the simulation cells – at least for the considered dimensions of the periodic simulation cells (few nm) corresponding to few thousands atoms (i.e. well above the insolubility limit). This somehow invalidates the concept of molecular model, defined as an assembly of unbound molecules, for this types of kerogen[15,61]. In the case of O-rich kerogen (type III), the REMD simulations by Atmani et al.[16,79] and Leyssale et al.[17] have shown that while kerogen may be composed of few moderate weight (few thousands Da) molecules at low maturities – which may also result from oversimplified OM models –, it quickly evolves to a unique cross-linked entity during maturation.

2.3.3 Density and porosity

Kerogen is a multiscale and heterogeneous material, with a multiscale porosity ranging from the nanometer to the micrometer, as can be assessed from gas adsorption and small angle neutron scattering.[88–91] To build the atomic kerogen models that are the subject of this review, one of the most important parameters is the density at the $\sim$ 5-nm scale. This is fundamental, as it is directly correlated to the porosity of the models as well as their mechanical, adsorption and transport properties. However, the intrinsic density of OM at this scale can be difficult to assess because of the small pores present in the samples and the fact that they always come embedded with inorganic matter.[88,89,91] Nevertheless, it is commonly accepted that densities in the range $0.9-1.4$ g/cm^3 are to be expected, depending on kerogen maturity and burial depth of the deposit.[36]

In the case of molecular models, the density of the final 3D model is both an input and an outcome of the relaxation, because it depends on the number of building block molecules[49] and fluid molecules[51] (or dummy particles[49,50,52]) used, and the applied temperature/pressure conditions.[92] Note that despite the introduction of large (up to 40 Å) dummy particles to force a mesoporosity, upon their removal the 3D structure always relaxes and partly fills the created voids, allowing reaching a maximum pore diameter of $\sim$ 20 Å independently of

the number or size of spacer particles introduced.[49,52] This maximum pore size would be $\sim$ 8 Å at 1 bar and 298 K without any fluid or dummy particles, with decreasing values for larger pressures.[49,50,52] For IG, QMD, and HRMC models, density is imposed at the beginning of the simulation by the number of atoms placed in the simulation box of a fixed size. The most representative samples are then chosen between the different models produced as the ones that best reproduce some other quantities, such as pore size distribution or bulk modulus.[15] Finally, REMD models are special in the sense that the density is an outcome of the simulation, that mainly depends on the pressure/temperature conditions and the maturity of the samples. In these models, the porosity appears when a fluid is produced, i.e. mainly water, carbon monoxide, dihydrogen, methane, and methanol (in decreasing concentration for lignin-based kerogen).[16] The final density was also shown to depend on the type of OM at the origin of the produced kerogen, and whether some of the produced molecules were expelled (i.e. removed) during the simulations. Densities in the range 0.6–1.3 g/cm^3 were obtained for type III kerogen deriving from cellulose[16,79] and lignin.[16,17]

2.3.4 Mechanical properties

As will be discussed in section 3.1, the mechanical properties of kerogen are particularly important ones, as (i) the ability of the kerogen to deform (swell) upon adsorption is intimately linked to its elastic properties,[61] and (ii) the efficiency of the hydraulic fracturing is correlated to its fracture behavior. Using nanoindentation on kerogens of various maturities, it was shown experimentally that kerogen stiffness is positively correlated with maturity, with the Young's modulus increasing from roughly 3 to 10 GPa.[93] This is an expected correlation, as the sp^2 carbon content as well as cross-linking increase with maturity, which results into an increased mechanical resistance. This positive correlation between maturity and stiffness was also obtained for the QMD[61] and HRMC models.[15] Moreover, using HRMC models, Bousige et al. also showed that, at fixed maturity, all elastic moduli increase with the density of the models.[15]

Mechanical studies using molecular models[94,95] also found a positive correlation between density and stiffness. However, a negative correlation between maturity and stiffness was obtained, conflicting with both the simulations of Bousige et al.,[15] the experiments of Wang et al.,[93] and intuition: the stiffest kerogen should be the one with the stiffest elements (aromatics) and the largest degree of cross-linking, namely the most mature kerogen. This highlights a fundamental difference in stiffness buildup between the molecular and statistical mechanics based models. In the former, owing to the low molecular weight, which furthermore is independent from maturity, stiffness (and strength) results from non-bonded interactions (van der Waals and electrostatic forces, hydrogen bonds, entanglements, etc.) which overall are stronger in immature systems. Conversely, in the highly cross-linked statistical mechanics based models, stiffness and strength arise mostly from the covalent bond network of the carbon skeleton, which strength increases with increasing maturity.

The same reasoning applies to the fracture properties. Using their HRMC models, Bousige et al. were able to observe a crossover from a ductile behaviour for immature samples to a brittle behavior for mature kerogens, as evidenced by the shape of the stress-strain curves and the spatial distribution of the bond breakings observed: uniformly distributed for the immature case, and along fracture planes for the mature case.[15] Using molecular models, it was shown that the fracture surface depends on kerogen type,[95,96] with a smooth fracture surface for type III and a rough entangled fracture front for type I kerogen. All kerogen types were nevertheless shown to have a ductile behavior in those studies, yet one should be careful when concluding on those fracture properties, computed for low molecular weight non-cross-linked molecular models, and using non-reactive force fields – meaning that they cannot capture the rupture of covalent bonds.

Finally, while we are not aware of any mechanical evaluation of IG kerogen models, the bulk moduli – the isotropic measure of stiffness – of REMD models were also computed.[17,79] However, since in REMD models density and maturity are correlated, it is not possible to distinguish their respective correlations with stiffness. For instance, for lignin-based kerogen,

the bulk modulus K remains in the 0.7–3.2 GPa range when the H/C ratio evolves from 0.67 to 0.19, while the kerogen density decreases from 1.28 to 0.62 g/cm^3.[17] It has to be noted, though, that the largest value of K (3.2 GPa) was obtained for one of the most mature (H/C = 0.27) and less dense (0.62 g/cm^3) model, thus confirming the positive effect of maturity, in spite of the decrease in density.

2.3.5 Computational cost

Another critical point in the construction of atomistic kerogen models is the computational cost, i.e. the amount of computer resources and time required, which can be measured in terms of CPU hours spent to build the model. The construction of kerogen molecules and IG guided models comes at almost no computational cost, although some classical MD simulations have to be run to pack together several kerogen molecules to build a 3D periodic model (with or without a sacrificial porosity). This comes at a low price, of the order of 10^{3-4} CPU hours, which, with multi-threading, corresponds to a wall-clock-time of about a day. Despite the use of (more expensive) reactive force fields, the computational cost of the QMD models is similar to the one of molecular models. Yet, it depends significantly on the desired maturity: the more mature, the lower the quench rate, and therefore the longer the simulation. For the HRMC procedure, no multi-threading is possible due to the presence of the Monte Carlo steps. As the procedure requires a large number of MC steps to converge, especially for large systems as the number of steps scales with the number of atoms, the HRMC reconstruction can be pretty long, several months in terms of wall-clock-time for the 5 nm wide models in ref. [15]. However, as it runs on a single CPU, it remains relatively cheap in terms of computational cost ($\sim 10^4$ CPU hours). Finally, REMD is by far the most costly technique in terms of resources. This lead to computational costs of 1-10 million CPU hours per simulation. Note that an advantage of REMD is that models spanning maturities from immature to largely post-mature are obtained from one single calculation, which moderates the extensive computational cost of the technique.

2.3.6 Detailed structure comparison

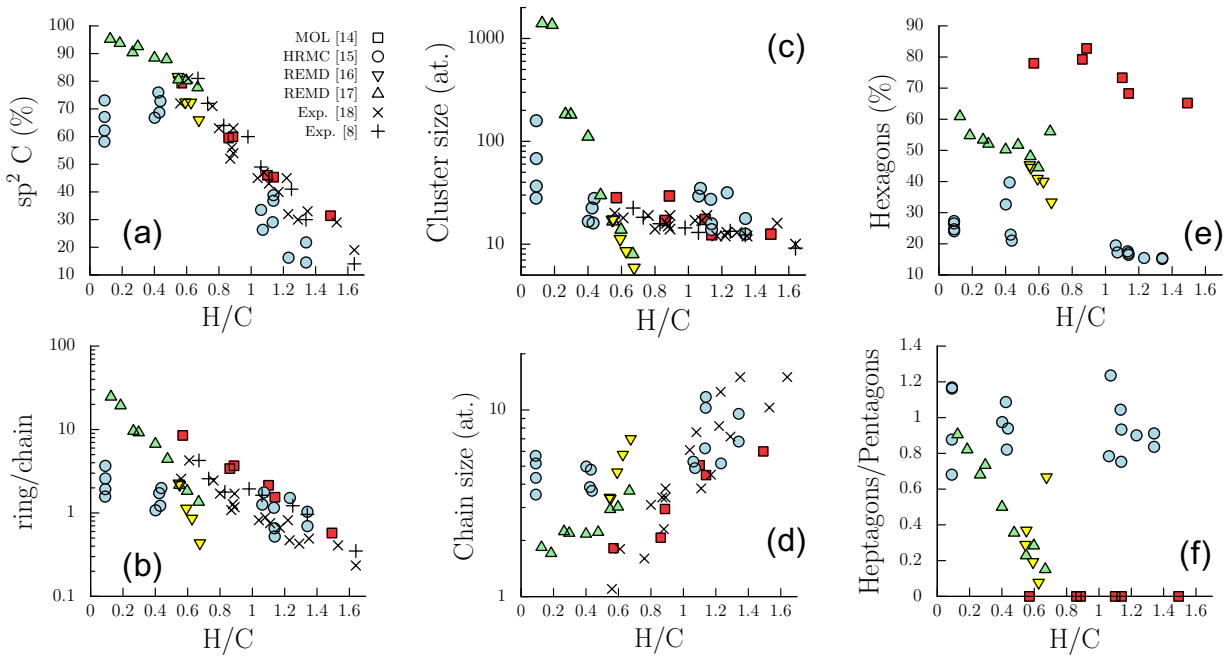

Figure 3: Comparison of some chemical, structural and textural features of three different classes of atomistic kerogen models: the molecular models of Ungerer et al.[14] (squares), the reconstructed HRMC models of Bousige et al.[15] (circles) and the mimetic REMD models obtained from cellulose by Atmani et al.[16] (down triangles) and from lignin by Leyssale et al.[17] (up triangles). Displayed properties are (a) the number of sp^2 carbon atoms, (b) the ratio of the number of heavy atoms (C and O) belonging to a ring to the ones belonging to a chain, (c) the mean size of clusters of connected rings, (d) the mean chain size between aromatic clusters, (e) the percentage of heavy atoms in hexagons and (f) the ratio of the number of heavy atoms belonging to heptagons to the ones belonging to pentagons. All theses properties have been computed using the procedure described in ref 16 and are shown as a function of the H/C ratio – as a measure of maturity. Note that for these calculations, N and S atoms of the molecular models were replaced by C and O atoms, respectively. Also shown on the figure are comparable experimental data extracted from Kelemen et al.[18] (crosses) and Béhar et al.[8] (pluses).

To complete this section, we present in Fig. 3 a comparison of four series of kerogen models belonging to three important classes of models: molecular,[14] HRMC reconstructed,[15] and REMD mimetic.[16,17] For these different systems, we have applied the method described in ref. [16] to compute a series of properties characterizing their chemistry (sp^2 carbon fraction), the local structure of their ring content (ratios of hexagonal, pentagonal and heptagonal

rings), and their texture (ratio of heavy atoms in ring structures to those in chain-like structures as well as the average size of ring clusters and chain-like clusters). Recognizing that the atomic H/C ratio decreases smoothly upon maturation (see Fig. 1) and that it is also naturally associated with texture evolution – H/C evolves from ~ 2 for pure unsaturated aliphatic chains down to ~ 0 for a pure aromatic system with large graphenic domains – we use here this ratio as a straightforward measure of maturity. At first glance, all types of models are able to capture some important trends that are seen experimentally, namely that with decreasing H/C ratio (i.e. increasing maturity), (i) the sp^2 C content increases, (ii) the relative content of atoms (C and O) in rings with respect to those in chains increases, and (iii) the size of the ring clusters increases while the one of chain-like clusters decreases.

Looking more closely at Fig. 3a, we see that most models seem to follow the almost same evolution path, in agreement with the existing experimental data, for the sp^2 content, which is clearly an excellent validation of the HRMC and REMD models (we recall here that the sp^2 content is imposed in the molecular models). The only series of models that significantly deviates from the rest of the data is the set of overmature PY02 HRMC models for which the sp^2 content seems underestimated. This may be due to significant amounts of cumulene (sp) carbon chains in these models.

Regarding the texture (Fig. 3b-d), clear evolution trends, common to almost all modeling and experimental data, can be observed. The ring/chain ratio plotted in logscale (Fig. 3b) evolves almost linearly with H/C (increasing when H/C decreases). As for the sp^2 ratio, only the PY02 HRMC models appear as slight outliers, for the same reason. The increase in ring cluster size (Fig. 3c) and decrease in chain-like cluster size (Fig. 3d) with decreasing H/C is also well reproduced by all models.

The most noticeable difference between the various models is found when analyzing the size of rings in ring clusters. In Ungerer's molecular models, the fraction of hexagons (Fig. 3e) increases from about 65% for immature models to about 82% for mature models, the remaining rings being exclusively pentagons (Fig. 3f). Fractions of hexagons are significantly

lower in both HRMC and REMD models. Values increasing from $\sim$ 15% for immature to $\sim$ 30% for post-mature kerogen were obtained for the HRMC models, which may be low considering that expected rings mostly range from pentagons to heptagons with an expected majority of hexagons. In REMD models, highly scattered values, between 30 and 60%, are obtained in the early stages of the simulations when the kerogen starts forming (H/C $>$ 0.6) then slowly increases up to $\sim$ 60% for postmature kerogen. The ratio of the number of heptagons over the number of pentagons, shown in Fig. 3f is a good indicator of the curvature of aromatic domains, values close to unity correspond planar structures associated to graphene grain boundaries or point defects (Stone-Wales defects), while lower values indicate positive curvature (fullerene-like).[17] As discussed above, heptagons are absent from the molecular models and pentagons only found at the boundaries of aromatic domains, which is somehow unrealistic. Conversely, in the HRMC models, the heptagon/pentagon ratio remains fairly close to unity for all models, whatever their maturity. Instead, in the REMD models, this ratio increases from almost zero in the early stage of the simulation at which rings are not yet clustered, to almost unity when large and flat clusters dominate.

3 Fluid Thermodynamics and Transport in Kerogen

3.1 Fluids nanoconfined in Kerogen

3.1.1 Structure/composition relationships

With available kerogen models, several authors have considered the impact of kerogen's nanoporosity on the adsorption of alkanes – starting from methane up to longer chains such as dodecane.[15,97–102] When considering microporous kerogen models (pore size $<$ 2 nm) such as those obtained using the different methods discussed in the previous section, one invariably observes type I adsorption isotherms. Such classical adsorption type is characterized by a rapid pore filling at low pressure, followed by a saturation plateau at large pressures when

the porosity is saturated in adsorbed molecules. As expected, such adsorption isotherms were found to be reasonably described using Freundlich or Langmuir adsorption equation.[97,100] Noting n the adsorbed amount per mass of sample and P the gas pressure, the Freundlich model describes that $n \propto P^{1/n}$ while the Langmuir one assumes that $n \propto \alpha P/[1+\alpha P]$. Beyond such mathematical formulas, the essential difference between the two models is that the Freundlich model is empirical while the Langmuir one can be derived from robust thermodynamics or statistical mechanics grounds. For the former, we note that both asymptotic limits are nonphysical as the limit in $P \to 0$ fails to recover the Henry regime, $n \propto P$, while the limit $P \to \infty$ does not capture adsorption saturation.

Using the molecular models proposed by Ungerer et al.,[14] Alafnan et al. investigated in a couple of papers the impact of kerogen type and maturity on gas adsorption in their nanoporosity (here, we recall that nanoporosity is used to refer to pores at the nm scale which is often referred in the literature as microporosity, i.e. pore size < 2 nm).[98,99] By considering descriptors such as porosity, density and pore size distribution, these authors attempted to establish some structure/property relationship for methane adsorption. In particular, while they found an expected linear relation between the gas adsorption capacity and kerogen porosity, they showed that kerogens of type III possess the highest adsorption capacity followed by II and I. Moreover, for a given kerogen type, the adsorption capacity increases with increasing maturity as a result of the larger porosity being formed over time.[98] The same authors also proposed that traditional engineering models fail to quantitatively assess the gas-in-place as they do not consider both the adsorbed and free gas contributions. By considering different kerogen models (i.e. of different maturities), they also proposed that the number of double carbon bonds and type of heteroatoms (O, S, and N) affect the kerogen nanoporous structure and hence their methane adsorption capacity.[98,99]

Using their HRMC models, Bousige et al. investigated adsorption in kerogen's nanoporosity as a function of its type and maturity.[15] In this work, both N_2 adsorption at low pressure at 77 K and methane adsorption at 450 K in the high pressure range were studied – while

the former corresponds to a routine technique to characterize porous materials, the latter is relevant to gas recovery from gas shale at a characteristic burial depth. While the density of kerogen is often poorly known (kerogen samples usually include minerals that cannot be fully removed in experimental pre-treatments), the authors showed that the density to be considered in a numerical model can be constrained against available nitrogen adsorption data. Moreover, these authors also showed that the maturity is a key parameter in predicting the gas adsorption capacity, as shown in Fig. 4 by considering different kerogen types at the same density, the porosity was found to increase with maturity with a large impact on the methane content. Using the same kerogen models, Wang et al. investigated methane in local micropores.[103] By considering four sample types with different porosities/densities, they showed that the pore adsorption capacity decreases with pore size d in an exponential fashion as a result of the decreasing surface-to-volume ratio S/V in pores of increasing size (in fact, strictly speaking, we note that the adsorption capacity should decay as $1/d$ as does S/V).

In an attempt to move towards shale gas recovery, molecular models were also considered to investigate the gas content in kerogen in practical conditions. As shown in Fig. 4, Wu et al. studied methane adsorption in type II kerogens at different maturities while treating both the temperature and pressure as functions of the burial depth.[92] They found a maximum capacity at a depth of 1–3 km, consistent with practical observations. In agreement with other observations on different sample types and maturities, it was also found that the porosity change does not correlate directly with an adsorption change. This result suggests that the surface evolution in time – i.e. as the pressure and temperature vary when the sample gets buried deeper and deeper – is significant with a strong impact on the gas trapped in the kerogen's porosity. As another illustration of practical application of kerogen models, Huang et al. considered adsorption in a structure that mimics the kerogen found in Chinese Cambrian gas shale.[104] This molecular model, which is made up of kerogen macromolecules, bitumen components and residual lighter components, was found to capture some important

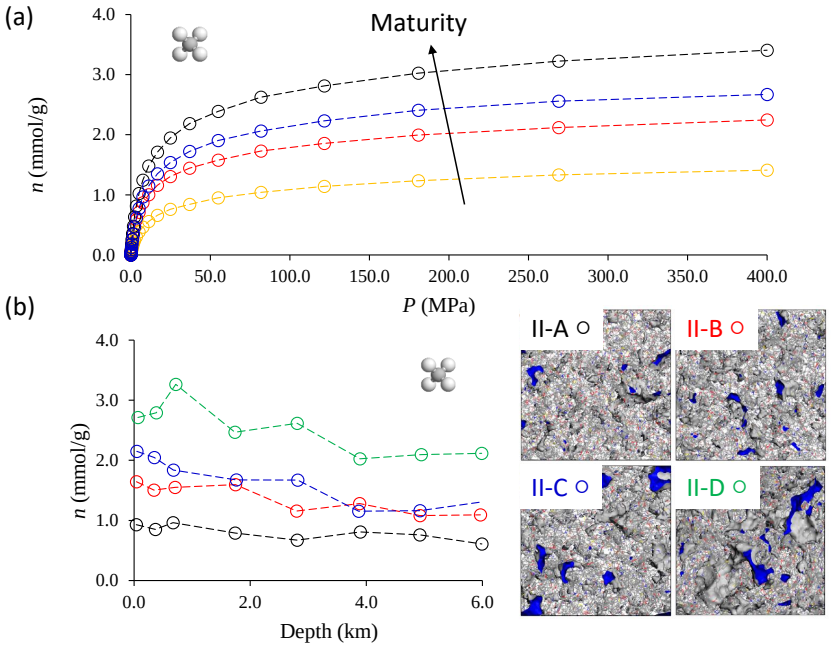

Figure 4: (a) Simulated methane adsorption isotherm at 450 K for 4 kerogen samples of density 1.2 g/cm^3.[15] The color code, which corresponds to kerogens of increasing maturity as obtained using HRMC, is as follows: MEK (yellow), EFK (red), MarK (blue), and PY02 (black). (b) Methane adsorption isotherm as a function of burial depth for 4 different molecular models of type II kerogen.[92] Snapshots of the models (reproduced – and adapted – with permission from ref 92. copyright 2022 American Chemical Society) are shown on the right for the sake of clarity.

physical parameters of the experimental sample. By considering the distribution of micropores (< 2 nm) in this system, these authors showed that gas molecules get adsorbed in a different fashion depending on the pore size and presence of heteroatoms.

Several authors have also studied the impact of kerogen's nanoporosity on the co-adsorption of alkanes (by considering the shortest alkane – methane – to longer chains such as hexane, nonane, dodecane, etc.). In particular, using molecular kerogen models, Wu et al.[105] and Zhang et al.[106] determined the excess properties and selectivity of kerogen for the adsorption of methane/ethane mixtures. In an effort to provide a thermodynamic framework to alkane co-adsorption in kerogen's porosity, other authors have considered different formalisms. Collell et al.[101] considered both the ideal adsorbed solution theory by Myers and Prausnitz,[107] which is a cornerstone in the modeling of mixture adsorption in chemical engineering, and the extended Langmuir model. While both models were found to describe reasonably the simulated adsorption isotherms at low pressure, these authors found that the agreement at high pressure only applies to kerogen with the largest micropores. In a similar spirit, Glatz et al.[108] considered additional adsorption models to describe methane/ethane co-adsorption in kerogen, namely the non-revised Langmuir, revised Langmuir, extended Freundlich, and Langmuir ratio correlation (with the latter providing the most accurate description of the data in case of mixtures). Using configurational-biased grand canonical Monte Carlo simulations, Falk et al.[102] considered the adsorption as well as the conformational structure of n-alkanes in a HRMC activated carbon model – that was used as proxy for kerogen. In fact, this model has a very similar porous structures to the mature HRMC kerogen models. While all n-alkanes were found to adsorb in low density kerogen, some size exclusion effects in the high density kerogen structures lead to low adsorbed amounts for long alkanes. Moreover, adsorbed alkanes adopt distorted configurations with respect to their bulk counterpart, therefore leading to a significant negative term due to the intramolecular contribution in the overall isosteric heat of adsorption.

3.1.2 Impact of wetting and Enhanced Oil Recovery

As far as molecular simulation studies using kerogen models are concerned, one of the first works on the impact of water on the thermodynamics of shale gas was performed by Lee et al.[109] In this work, the authors employed a free energy technique – the so-called umbrella sampling method – to determine the confinement and extraction of methane from kerogen models through a wet interface (both a membrane of carbon nanotubes and a HRMC activated carbon were considered). Such a recovery process through a flooded interface was found to involve a free energy barrier, therefore leading to activated transport during the extraction step. Later, Zhang et al.[110] also employed the umbrella sampling technique to investigate the interactions of oil with kerogen surfaces in the absence and in the presence of water. Using a more realistic kerogen surface, which includes surface groups, these authors showed that the minimal energy required to recover oil molecules significantly decreases at the kerogen surface if water is present. In parallel to these works on the impact of surface wetting on shale gas behavior in kerogen, several groups have used kerogen samples with preloaded water amounts to investigate the impact of moisture content on methane adsorption.[111–113] It was found that the methane adsorption capacity decreases with increasing the moisture content. This result is fully consistent with previous findings[114] on the impact of moisture content on the adsorption of methane or carbon dioxide in activated carbons. In particular, Ren et al.[112] found that the methane adsorption capacity decreases linearly with moisture content as water occupies the pore volume available for methane confinement/adsorption. However, for an immature type II-A kerogen, we note that Chong et al.[115] found that water possesses the largest uptake compared to methane and carbon dioxide owing to the strong water-kerogen interactions in such immature samples.

Several authors also considered the impact of moisture content on the co-adsorption of gases, typically, CH_4/CO_2 mixtures.[116,116–118] As illustrated in Fig. 5, using four kerogen molecular models of different maturities, Huang et al.[116] investigated the adsorption of CH_4, CO_2 and their mixtures in kerogens as a function of moisture content. Upon increasing

the moisture content, the CO_2/CH_4 selectivity was found to increase for the two mature samples and the most immature sample but to decrease for one of the immature sample. Such a result, which deserves further investigation to fully understand the role of moisture content as a function of the kerogen type and maturity, suggests that the impact of moisture content is driven by the water/kerogen interactions but also the gas/water interactions and porosity of the kerogen sample. As an interesting extension of these works on the role of moisture content, Li et al.[117] also considered the impact of water content and salinity on CO_2 injection in shale to foster methane recovery. Using a molecular model of type II-D kerogen, these authors considered the following thermodynamic conditions: 0–5 wt% moisture, 0–6 mol/L NaCl saline, and 0–5 wt% C_2H_6 at different temperatures and pressures. In line with the previous cited works, moisture content was found to be detrimental to CH_4 adsorption. Moreover, salinity and the co-adsorption with ethane were found to further decrease adsorption. Finally, while this will be discussed in more detail in the section below dedicated to poromechanical effects in kerogen, we note here that Huang et al. also considered the role of moisture content on the deformation of kerogen structures upon methane/carbon dioxide co-adsorption.[116,118]

In the rest of this paragraph, we briefly review the use of kerogen models to address the important problem of enhanced gas recovery through the injection of CO_2 in gas shales. For a more detailed review, the reader is referred to the recent review paper by Omari et al.[119] on theory, experiments and simulations on such a technical aspect. In an attempt to mimic enhanced gas recovery, Lee et al.[109] employed umbrella sampling to investigate the substitution of water by carbon dioxide to stimulate the extraction of shale gas. Using a simple model of kerogen in gas shale, in agreement with experimental observations, these authors found that replacing methane by CO_2 is favorable from a thermodynamic viewpoint owing to the strong interactions between CO_2 and kerogen. Since then, by investigating methane/carbon dioxide co-adsorption in molecular models of kerogen, many simulation studies have shown that injection of carbon dioxide indeed shifts the adsorption isotherm conditions by favoring

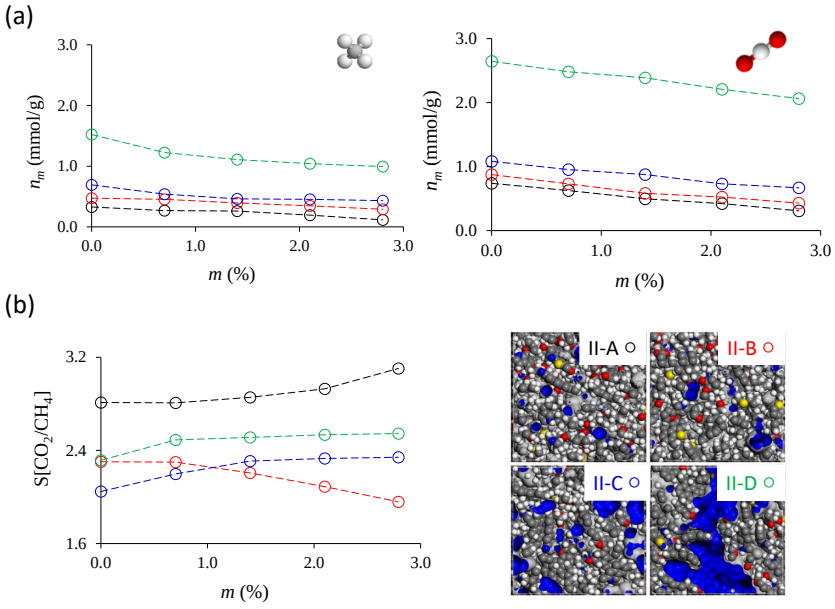

Figure 5: (a) Simulated maximum methane (left) and carbon dioxide (right) adsorbed amounts for 4 molecular models of type II kerogen as a function of moisture content m. (b) CO_2/CH_4 selectivity for the same kerogen molecular models shown in (a). We also show the 4 different molecular models of Ungerer et al.[14] Adapted and reproduced (snapshots) with permission from ref 116. Copyrirght 2017 Elsevier Ltd.

the depletion of methane.[120–125] While the thermodynamic view derived from these works should be complemented by transport coefficients (to fully grasp the complexity of enhanced gas recovery), they already provide a comprehensive view of the problem. Using similar molecular modeling approaches, other authors also considered simple available thermodynamic models to describe methane/carbon dioxide co-adsorption in kerogen.[108,126] Finally, as an important development beyond thermodynamic modeling, Xu et al.[127] have proposed a kinetic model of enhanced gas recovery. In more detail, using MD simulations describing the diffusion and displacements of gases involved in these processes, these authors derived an analytical model depicting the dynamic recovery in the kerogen matrix from the recovery time and capacity.

As briefly mentioned above, some authors also considered the impact of the presence of water (i.e. moisture content) on the co-adsorption of CO_2 and CH_4. In particular, Huang et al.[118] found that, despite a decrease in the the CO_2/CH_4 adsorption capacity, the CO_2/CH_4 adsorption selectivity increases with increasing moisture content, therefore offering perspectives to boost CO_2-enhanced gas recovery using moisture conditions. Other works available in the literature have included some additional complexity or specificities when modeling enhanced gas recovery using kerogen molecular models. By considering a molecular model of kerogen in Chinese Cambrian gas shale, Huang et al.[104] showed that the adsorption capacity is larger for carbon dioxide than for methane. Wang et al.[128] also considered CO_2 enhanced recovery but for the more complex situation of multi-component shale gas recovery (typically, CH_4, C_2H_6, and C_3H_8). Moreover, several authors have also considered the impact on enhanced gas recovery of kerogen swelling as methane gets replaced by carbon dioxide.[129,130] Finally, while this is out of the scope of the present review paper focused on kerogen models only, we note that some authors have also investigated by means of molecular simulation the co-adsorption of CO_2/CH_4 on heterogeneous shale surfaces made up of organic and mineral parts.[109,131]

3.1.3 Poromechanics: sorption-induced deformation

While the mechanical properties of kerogen were discussed in section 2, we consider here sorption-induced deformation of kerogen. Reviewing the experimental literature is out of the scope of the present paper but we emphasize that there are numerous examples of sorption-induced swelling,[132,133] one also reporting a molecular dynamics study of the differential swelling when different fluids are considered.[133] From a theoretical viewpoint, in their seminal work, Ertas et al.[134] derived an extended Flory-Rehner and regular solution theory model to describe the swelling of kerogen in contact with solvents. These authors showed that the swelling induced by the confinement of a fluid in kerogen's porosity is driven by thermodynamic and structural parameters: solubility parameter, cross-link density, and volume fraction of the kerogen network. These authors also proposed that the equilibrium composition of molecules retained in kerogen can be predicted provided the composition of the mixture in the reservoir is close to that initially contained in the kerogen. Later, Obliger et al.[61] performed explicit molecular simulations of kerogen swelling for an immature type I kerogen model as a function of temperature, external pressure and methane loading. Using two typical kerogen models (an immature model with H/C = 1.1, and an overmature model with H/C = 0.1) produced by QMD, they also carried out extensive MD simulations to determine the evolution of the poroelastic properties of kerogen structures under various conditions relevant to shale gas recovery. As expected, their results show that immature kerogen is highly deformable while overmature kerogen remains quite stiff (so that the rigid framework approximation holds reasonably for the latter). By considering the poromechanics framework first introduced by Coussy[135] and then extended by Brochard,[136] these authors showed that the adsorbed amount n in swollen immature kerogen does not obey the linearized version proposed by Brochard, i.e. $n = n^0(1+C\varepsilon)$ whith n_0 the adsorbed amount in the non-swollen sample. Overall, for the specific conditions considered, owing to such deformability aspects, it was observed that the density can vary by a factor 2 with an accessible porosity increasing concomitantly from 0 to $\sim 30\%$. The linearized microporomechanical framework

introduced by Brochard et al.[136] was also used by Huang et al.[137,138] to consider the effect of preloaded water – to mimic the impact of moisture content – on the swelling of kerogen subjected to CH_4/CO_2 co-adsorption. These authors proposed that enhanced gas recovery can be maximized by tuning the the reservoir moisture as well as CO_2 injection conditions. However it has to be noted that important parameters, like the bulk modulus of the kerogen models and the poromechanical coupling constant (C) entering in Brochard's model, were directly taken from Brochard et al.,[136] although these constants are supposedly dependent on the porous material, gas, and thermodynamic conditions.

Besides the works above, most studies on adsorption-induced deformations of kerogen involved a direct mimetic approach, in which a grand canonical MC algorithm is combined with simple MD simulations in the isothermal-isostress (NσT) ensemble. Such hybrid simulations probe the adsorption of fluid molecules from the external environment imposing a given chemical potential and temperature, while allowing for mechanical deformations due to the external stress applied to the system. Such an external stress can correspond to the constraint exerted by the adsorbing pressure – the so-called "drained (or unjacketed) conditions", in which case the external stress corresponds to the negative of the fluid pressure – or to an external mechanical constraint imposed by the surrounding medium – the so-called "undrained (jacketed) conditions", in which case the external stress is not related to the fluid pressure but to the geological medium surrounding the system. As a typical example of drained adsorption, such a combined MC/MD simulation strategy was used to investigate the swelling of kerogen including some mesoporosity containing either gas or liquid hydrocarbons.[52] As expected, smaller hydrocarbons in both the gas and liquid phases were found to possess a larger adsorption capacity. Interestingly, by considering hydrocarbon at conditions corresponding either to the gas or liquid phase, the authors also established that the so-called Schroeder's paradox – an important observation that polymers swell more in the liquid phase than in the gas phase – also applies to kerogen-hydrocarbon systems.

3.2 Fluid Diffusion and Transport

The first paper explicitly addressing the MD simulation of transport in kerogen using an atomistic model dates back to 2015.[139] There, the authors considered an HRMC activated carbon model, as a reasonable proxy for mature kerogen. Prior to that, diffusion in such carbon model was investigated at low temperature (77 - 120 K) to show that the self-diffusion coefficient (or self-diffusivity) exhibits a maximum with fluid loading typically around 45-65% of fluid loading.[69,140,141] However, at larger temperatures ($\geq$ 300 K), diffusion decreases monotonically with the fluid loading.[142]

Falk et al.[139] showed that the usual Darcy's law is not valid to describe the transport of linear alkanes (from methane to dodecane) in kerogens due to strong adsorption effects. In fact, the linear response between pressure gradient and flow holds, but the proportionality coefficient is not simply given by the permeability of the porous structure and the viscosity of the fluid, instead, it was found to depend on the fluid density, etc. Such a result is due to the fact that the fluid adsorbed in such amorphous and confining media cannot be treated independently from the kerogen itself (there is no bulk or free fluid). As a consequence, hydrodynamic modes within the fluid do not develop, making the notion of viscosity inappropriate in this case.[139]

More generally, collective effects can be neglected on the long term diffusion, the self and the collective diffusion coefficients are thus approximately equal. The transport properties can then be determined from the self-diffusion coefficients that are simply obtained by equilibrium MD. Also, the transport properties of the alkanes scale as the inverse of the number of monomers in the alkane molecule and decrease with fluid concentration (see Fig. 6a). Then, those conclusions have been generalized[143] for alkane mixtures in Bousige's PY02 HRMC kerogen model[15] – which is structurally and chemically very similar to the activated carbon model mentioned above. On top of being able to neglect the collective effects within the same species of the mixture, it was shown that cross diffusion between species can be neglected and that the transport properties of the species can also be determined from their self-diffusion

coefficients. In the end, the transport properties only depend on global properties of the adsorbed fluid mixture such as the concentration of alkanes' monomers regardless of the fluid composition.[143] In the studies above, carbon microstructures were treated as perfectly rigid frameworks. As such, due to the exponential decrease of the available free volume with the quantity of adsorbed fluid, the transport properties decrease as well. This trend has been rationalized using a free volume theory[139,143] which introduces two parameters: a friction coefficient ξ_0 that controls the diffusion of a single alkane monomer (or methane) in the infinite dilution limit and a free volume parameter α that controls the decrease of the diffusion coefficient with that of the free volume. For n-alkanes (from methane to dodecane) in a kerogen model, it was shown that a single pair of values for those parameters is sufficient to describe the transport properties of alkanes' mixtures – regardless of the composition of the fluid thanks to the noticeable absence of collective effects on transport within the adsorbed fluids.[143] This free volume scaling appears to hold whenever the porosity is ultra-confining, i.e. both disordered and microporous. Also, the required coefficients (ξ_0 and α) are directly correlated with the pore volume fraction of the kerogen microstructure.[144]

Meanwhile, interpretative molecular models were widely used to investigate their transport properties, starting by one kerogen model of Ungerer et al.[14] The type II-C kerogen model (see Fig. 2c) was used to study the transport properties of a model condensate-rich gas mixture.[145] It was shown that transport can be considered as purely diffusive, e.g. correlations between fluid molecules can be neglected so that the self-diffusion coefficients of each fluid species can be used to predict their transport coefficients. In addition, the transport properties of linear alkanes scale as the inverse of their chain length. Within a similar type II model, Wang et al.[120] report decreasing trends with the adsorbed fluid quantity for the self-diffusion coefficients of methane and carbon dioxide within binary mixtures of various CH_4:CO_2 molar proportions, 1:1 (see Fig. 6b), 1:2, 1:3, and 1:4, with the diffusion of CH_4 being always slightly larger than the one of CO_2, as also noticed in ref. [147]. Such difference can be explained by invoking the difference in isosteric heat of adsorption between these

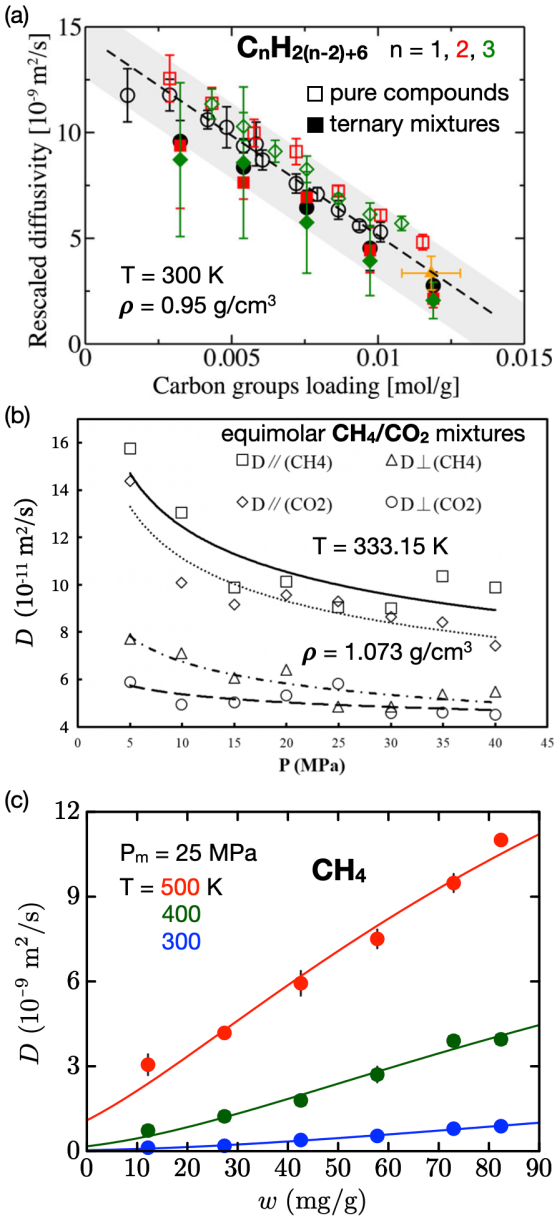

Figure 6: (a) Self-diffusion coefficient of linear alkanes in a type II-C kerogen (see fig. 2c) scaled by an optimal parameter that is close (but slightly superior) to the number of carbons of the alkane, as a function of the fluid loading in mole of carbon per gram of kerogen matrix (reproduced with permission from ref 145. Copyright 2015 American Chemical Society). The dashed line corresponds to a linear scaling. (b) Self-diffusion coefficient of methane and carbon dioxide in equimolar mixtures adsorbed in a type II-A kerogen, as a function of the hydrostatic pressure (reproduced with permission from ref 120 under a CC BY licence. Copyright 2017 by the authors). Diffusion is slower in one of the three directions. Lines are a guide for the eyes. (c) Self-diffusion coefficient for methane adsorbed in a QMD model of immature type I kerogen, as a function of the fluid loading in milligram of fluid per gram of matrix (reproduced with permission from ref 146. Copyright 2022 American Chemical Society). The mechanical pressure P_m is applied to systems where the fluid loading is imposed to mimic geological conditions. The lines correspond to a free volume model accounting for the swelling.

fluids. Significant anisotropy was also reported due to the size of the cubic simulation box ($\sim$ 3.3 nm).[120] Type I-A molecular model has been considered by Yu et al.,[148] who found methane diffusion to be considerably larger than in the type II and III kerogens mainly because of the lower density of the type I microstructure. On a more fundamental side, Vasileiadis et al.[149] have introduced the concept of Limiting Pore Diameter (LPD) to find that diffusion in molecular models of type II-D correlates linearly with the LPD. Also, Perez et al.[150] used a type II-C molecular model to highlight that Graham's law – stating that the self-diffusion coefficients scale as the inverse of the molecular weight in gas condition – remains valid in ultra-confining conditions for a variety of molecules composing a black oil.

One of the common points of the examined literature is to overlook the poromechanical couplings between the adsorbed fluid and the kerogen microstructure, notably the adsorption-induced swelling that is modulated by the flexibility of the structure. In particular, it is thought that a more rigid structure (elastic, mechanically speaking) will be less prone to swelling than a flexible one (viscoelastic). Wu et al.[151] attempted to account for the flexibility effects on the transport properties of a molecular model of type II-A kerogen. They conclude that transport decreases with the adsorbed fluid quantity and even that transport is larger when the whole microstructure is rigidified. However, their results can be influenced by the methodology used to impose the mechanical constraints on the system, (i) in the direction in which the transport properties are studied, pressure is imposed by the fluid in the two reservoirs surrounding the kerogen (a boundary-driven method was used to simulate the pressure gradient), (ii) the size of the system is imposed on both directions perpendicular to the flow, and (iii) some atoms of the solid are arbitrarily frozen during the simulations. Specifically, the last two conditions prevent the swelling of the kerogen microstructure that can be important here, as pointed in ref. [121] for a molecular model of type II-C kerogen – in line with the fact that the kerogen molecules used in such models have masses below the insolubility limit. A simpler and more robust investigation of the adsorption-induced swelling on diffusion is given in ref. [152] in which the authors used a QMD model of immature type

I kerogen to simulate methane diffusion at various loadings under geological temperature and pressure and using undrained/jacketed conditions. In this kerogen, prone to important adsorption-induced swelling, methane diffusion increases with the amount of adsorbed fluid due to the accompanying free volume increase. It is also shown that, at constant volume, the effects of the internal motions of the kerogen matrix coupled to the dynamics of the fluid enhance the diffusion and that this enhancement is more important at low fluid loading because pore size fluctuations have a more dramatic impact on the pore connectivity than at high loading where the pore network is always well connected. Following on this work, Ariskina et al.[146] highlighted that kerogen flexibility do not promote significant collective effects on the diffusion. Again, as in the rigid case, the collective- and the self-diffusion coefficients are approximately equal and the latter can be used to predict the transport properties. It is shown that the increase in self-diffusion coefficient with increasing fluid loading – due to the important adsorption-induced swelling – can be further rationalized by the use of a free volume model (see Fig. 6c). However, this uncommon positive correlation between fluid loading and diffusivity due to adsorption-induced swelling may only be valid for immature kerogens for which adsorption-induced swelling is important.

3.3 Pore network effects: multimodal porosity, accessibility

In an attempt to describe the complex multiscale nature of kerogen, several authors have considered numerical models displaying multimodal porosity (i.e. kerogen structures that possess two or three porosity scales from the nanoscale to beyond). Typically, most authors simply consider nanoporous kerogen structures (pore size < 2 nm) which are combined to include a large mesopore ($2 - 50$ nm) as in ref. [153]. Using a similar approach, Tesson et al.[39] have also proposed such models of kerogen slit mesopores to study the impact of the microporous walls on the adsorption in the mesoporosity (Fig. 7a). In parallel, beyond the simple slit geometry, other authors have prepared kerogen bimodal structures by creating, within a kerogen model, pores of different shapes (cylindrical or square hole for instance).[126,154,155]

Such models were used to probe the impact of confinement on gas adsorption as it is known to vary drastically with pore shape/size. Finally, Michalec and Lisal[50] proposed a refined strategy to produce such multimodal kerogen models and investigate the confinement of pure methane and a mixture of 82% of methane, 12% of ethane and 6% of propane in kerogen. Using Ungerer's kerogen molecules, these authors used dummy atoms of varying size during the 3D structure generation to introduce micro- or mesoporosity.

From a thermodynamic viewpoint, using microporous/mesoporous kerogen models, simple bimodal kerogen models (i.e. microporous/mesoporous materials) have allowed gaining the following insights using molecular simulation. Huang et al.[156] showed that the large nanopores in kerogen are not saturated with methane at deep shale reservoir conditions. Using a more refined model (with mesopores of a more realistic morphology compared to the slit geometry coexisting with micropores), Perez et al.[150] observed that methane fills the pores while longer n-alkanes adsorb at the pore surface. Moreover, these authors found that such heavier alkanes adsorbed at the pore surface partially or completely obstruct the pore entrances in kerogen. Finally, using a simple kerogen model containing both the kerogen's intrinsic microporosity as well as a large mesopore, Falk et al.[102] investigated the different contributions of such bimodal porosities in the adsorption of alkanes in kerogen. First, depending on the alkane chain and temperature conditions considered, different adsorption isotherms are observed. Methane adsorbs in both porosities at all pressures with an adsorbed amount that increases in a continuous and reversible manner with pressure. Dodecane adsorbs at low pressures in the kerogen's nanoporosity before undergoing capillary condensation at a larger pressure, therefore leading to a discontinuous change in the adsorbed amount. Such a dichotomy is well-established in the field of adsorption: small pore (or equivalently large molecules) follow reversible and continuous filling, while large pores (or equivalently small molecules) exhibit capillary condensation. In fact, at a given temperature, there is a critical diameter below which pore filling and emptying no longer follows first order capillary condensation as observed for large pores. In agreement with

results for gas adsorption in hierarchical porous materials,[157,158] Falk et al. found that the overall adsorption isotherm simply is a linear combination of the adsorption isotherms in the different porosities (kerogen microporosity and larger mesoporosity).[102] Using kerogen models with external surface connected to a larger porosity, typically a mesopore acting as a reservoir of methane, several groups have also investigated the pore space accessibility in kerogen nanoporous structures.[15,50,102,159] By conducting MD simulations, instead of grand canonical MC simulations which allow fluid particles to be inserted/removed everywhere in the nanoporosity, these authors determined the amount of gas diffusing from the reservoir into the kerogen structure. In doing so, it is possible to assess the amount of porosity and, hence, of gas that can diffuse from/to the kerogen porosity. In particular, in the final equilibrium state, one readily obtains the amount of gas inside the matrix as a function of the gas pressure left in the reservoir. As a striking result, by comparing adsorption isotherms obtained with and without taking into account such accessibility issues for different mature and immature kerogens, it was found that pore connectivity is poor for all materials: about 80% of the pores are closed in immature models and about 20 to 60% in more mature samples[15] where experimental values for Barnett shales stand between 25 to 45%.[89] It should be noted that even if such molecular dynamics approaches are useful to probe accessibility aspects as well as kinetic effects in adsorption/desorption processes, they are limited to short time scales only. Indeed, by construction, due to limited computer power, regular MD simulations only probe timescales of the order of 1–100 ns, so that it only provides a lower limit of pore accessibility. In other words, it cannot be ruled out that some apparent inaccessible pores on short timescales would get filled at longer times. In this context, we note that free energy techniques, such as those employed in ref. [109], would provide a more complete picture by providing the free energy landscape for diffusion into the kerogen structures, which can be converted into characteristic transport coefficients in the framework of the transition state theory.[160] Also, we note that the flexibility of the kerogen structures, neglected here, can increase the accessibilty.

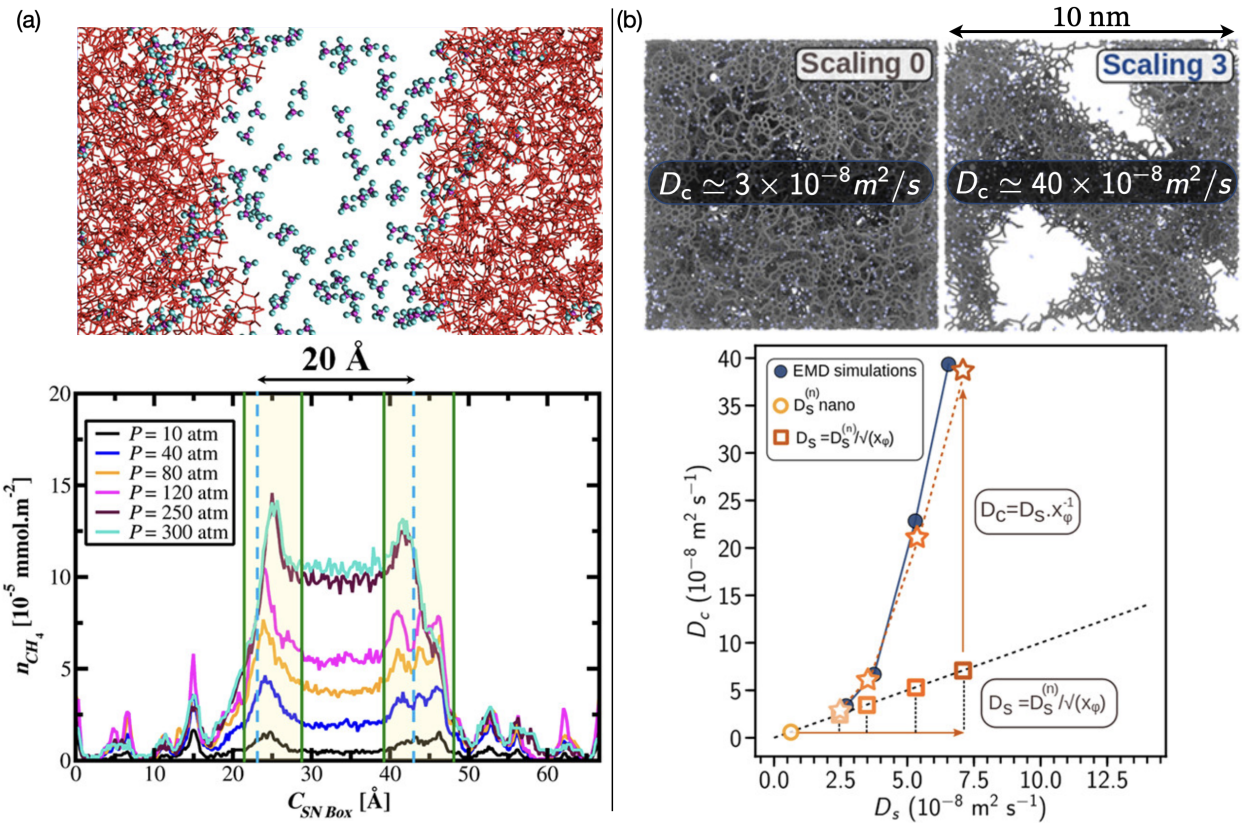

Figure 7: (a) Adsorption profile of methane within a slit mesopore created in a molecular model of type II-A kerogen. The atoms of the kerogen are depicted in red while those of the fluid are in pink for the carbons and blue for the hydrogens (reproduced with permission from ref 39. Copyright 2018 American Chemical Society). (b) Collective diffusion coefficient of methane as a function of the self-diffusion coefficient for dual-porosity systems where the mesoporosity is carved out of a QMD model of mature type I kerogen according to an image obtained by HRTEM. The 4 different systems correspond to different scaling degrees indicating the level of increase of the volume of the mesoporous phase so as to decrease the microporous fraction x_ϕ. The orange circle stands for the self-diffusion coefficient evaluated for the bulk microporous kerogen, the empty squares for the ones predicted by the $1/\sqrt{x_\varphi}$ scaling, and the empty stars for the estimate of the collective diffusion coefficients adding the $1/x_\varphi$ scaling that quantifies the collective effects on the diffusion properties. (reproduced with permission from ref 161. Copyright 2020 American Chemical Society)

Then, coming back to diffusion properties, Magnin et al.[161] extruded atoms out of QMD models of kerogen by mapping a part of a three dimensional electronic tomogram[162] so as to obtain kerogen models containing both the microporous and the mesoporous phases with a realistic geometry (Fig. 7b). By artificially increasing the fraction of the mesopores in the systems, they have shown that when the fraction of mesopores becomes more important than the one of the micropores the collective effects become non negligible as the collective diffusion coefficient becomes larger than the self-diffusion one. This is expected because the mesoporosity of such systems is connected through the periodic boundary conditions, so that collective effects can develop in the fluid which can flow across the system without having to diffuse in the microporous phase, even though sorption/desorption between the microporous structure and the mesoporosity is always possible. Interestingly, it has been found that the ratio between the upscaled self-diffusion coefficient and the self-diffusion coefficient of the microporous phase, scales as the square root of the microporous fraction of the total pore volume.[161] Furthermore, the ratio between the upscaled collective-diffusion coefficient and the upscaled self-diffusion coefficients scales linearly with the microporous fraction, thus allowing to predict the transport coefficient from the knowledge of the self-diffusion coefficient within the microporosity and the microporous fraction (Fig. 7b). In ref. [162], the electronic tomograms revealed mesopores that are mostly scattered among the microporous phase, meaning that fluid molecules have to adsorb in the microporous phase in order to diffuse across the kerogen. Thus, the study of transport focused on the upscaling of the self-diffusion coefficients. Continuous time random walkers simulations, accounting for different diffusion coefficients for the fluid in the mesoporosity and in the microporosity, have been used, allowing the fluid to diffuse through the interface between both porosities based on the ratio of fluid concentrations. The numerical results obtained for various kerogen mesostructures have been used to validate an analytical model predicting the upscaled self-diffusion coefficient as a function of the fluid concentrations and the self-diffusion coefficients of the fluid in the two phases, and this with the need of only one single effective parameter

accounting for the geometry of the mesostructure.

4 Perspectives

4.1 Towards better models

As discussed in section 2.3, all existing models present some varying degrees of inaccuracy – clearly leaving room for improvement. An ideal kerogen atomistic model should, (i) have the chemical accuracy of 3D molecular models, (ii) be large enough to provide a good statistical description, (iii) be cross-linked enough not to be soluble and capture the mechanical properties of the material (including their variations with maturity, density, etc.), (iv) capture the intrinsic multiscale porosity of kerogen, and (v), above the kerogen itself, models should also exist for the kerogen interfaces with inorganic matter in shale. Despite the significant efforts reviewed in this manuscript, there remains room for improvement for all types of model to reach these goals. We highlight here some possible research directions.

Although machine learning (ML) strategies such as those presented in ref. [40] could certainly improve the quality of molecular models, ML itself cannot solve the main drawbacks of such models, namely that they indeed are "molecular" models, and as such unable to capture the complexity of highly cross-linked materials such as kerogen. This statement is better understood in the overmature limit. Extrapolating the 250 C atoms molecular models to a higher maturity with $\sim$ 100 % of aromatic C would lead to a large polycyclic aromatic hydrocarbon. While this can maybe be a reasonable model of some coal tar pitches, this obviously cannot be one of overmature kerogen. That being said, strategies to turn molecular models into cross-linked ones, as was done with the image guided method,[59] remain promising, provided that the building blocks are diverse and numerous enough to provide a good statistical description of the kerogen.

A straightforward improvement pathway for reconstruction models would be attempting to reach a chemical quality similar to the one of molecular models. With that aim in mind,

an option to explore might be the recently proposed Hybrid Reverse Molecular Dynamics (HRMD) method,[163,164] in which a fictitious force field forcing the minimization of the error on $S(q)$ is imposed at each MD step on top of the regular reactive force field. The advantage of this technique is its rapidity compared to HRMC since multithread computation is possible in RMD (like in classical MD), whereas it is not possible in HRMC due to the occurrence of MC steps. It was successfully applied to carbon blacks with various degrees of order,[164] so that it should be readily applicable to kerogens of various maturities. To improve the distribution of chemical functions in these models, one could consider energy penalties based on some extended experimental target data like NMR spectra calculations. Similarly, pore size distribution, HRTEM image properties, etc. could be introduced in the reconstruction process, provided that the latter are easy and cheap to compute, to improve the structure/texture of the models.

Mimetic modeling could be improved by performing REMD with more realistic precursors and larger systems. Kinetic-based methods, rather than thermodynamic-based methods like REMD could also be considered. In this regard, Valdenaire et al.[165] have recently proposed a method based on first passage times and kinetic integration to accelerate the RMD simulation of cellulose pyrolysis. Although promising, the obtained gain in timescale was insufficient to consider such methods for geological evolution so far. Finally, improving the available reactive force fields will obviously be key to improved statistical mechanics based models. The ML force fields are becoming increasingly popular and, in the case of pure carbon systems, the gaussian approximation potential of Rowe et al.[166] has been shown to surpass the most popular empirical potentials in many aspects. Nevertheless, additional advances are required before such accuracy can be reached for more complex systems containing at least C, O and H atoms, and possibly N and S.

The natural inclusion of mesoporosity – as opposed to former studies where it is imposed via sacrificial spacers[49–52,151] or by cutting larger pores within initially microporous models[161] – is also a challenge that remains to be solved for more realistic and consistent (i.e. in the

sense that mesopores would not fall apart when removing the artificial dummy particles) micro/mesoporous models. Considering the discussions above, as long as their molecular weights stay on the low end, molecular models do not seem to be the most relevant ones here. However, mesoporosity should occur naturally in reconstructed or mimetic methods, provided that suitable simulation conditions are met. First of all, systems significantly larger than those of 5 nm or less used so far in HRMC or REMD simulations should be considered, raising a real issue with computational cost, especially for REMD. Asides from these practical considerations, HRMC/HRMD reconstructions should be performed at lower overall densities with additional constraints on the pore structure like small-angle X-ray diffraction or pore size distributions. In REMD, mesoporosity should also appear naturally, via a phase separation between the dense kerogen parts and bulk-like fluid areas. Note that early signs of mesopore developments were observed in ref. [17], yet the system size was too limiting to allow for large mesopores to appear.

Atomistic models of organic/inorganic interfaces in shale should also be developed allowing for detailed investigations of sorption and transport at those interfaces. These information would be crucial for upscaled models of shale systems thermodynamic and transport. Mechanics at these interfaces is also certainly intimately linked to the efficiency of the fracking process and, hence, to the efficiency of oil and gas recovery. Numerical investigations on the mechanical properties of kerogen/mineral composite systems would be valuable tools in this regard. So far only a few reports, with simplified kerogen models, have been published on this topic.[71,167]

4.2 Realistic models for gas adsorption and transport

An important challenge in the field of kerogen modeling and its applications for hydrocarbon adsorption and transport concerns the complex time and length scale dependence involved in these processes. Like vitreous systems in condensed matter physics, kerogen is an out-of-equilibrium, disordered material which evolves in time as it gets buried deeper and

deeper underground. As a result, the modeling of kerogen and, in general, of gas adsorption and transport in its porosity, opens the question of the complex underlying kinetics of these processes. Generally, when modeling kerogen structures, timescale separation is implicitly assumed. Considering the typical times corresponding to geological evolution, kerogens are assumed to be in a local equilibrium at the pressure and temperature imposed by the geothermal gradient at its location depth. While this appears as a robust approximation for molecular modeling, it raises the question of the evolution of kerogen materials and the gas trapped in their porosity as they are brought to external conditions that depart from those in situ. In particular, even if processes relevant to gas thermodynamics and transport in these complex materials occur in geological conditions, most characterization experiments against which molecular modeling is compared to are performed for very different external environments. For these reasons, in the field of kerogen modeling, important efforts should be devoted to investigate the behavior of gas adsorption and transport in kerogen under in situ conditions (i.e. as a function of external thermodynamic, chemical and mechanical conditions). In fact, with the aim to mimic potential evolution occurring in kerogen upon gas release/extraction, there is a need to develop models that allow considering operando conditions (e.g. temperature/pressure gradients, stress/strain constraints, and complex chemical environments).

Multiphysics aspects are another key challenge in the field of kerogen modeling to describe the thermodynamic and dynamical behavior of fluids in its porosity. In general, by multiphysics, we refer here to the complex interplay between thermodynamic, chemical, transport and mechanical phenomena that occur under most conditions in kerogen applications. In particular, considering the small scale porosity ($\sim$ nm) in kerogens, such coupling effects are expected to occur as the thermodynamics of the confined fluid leads to rich transport mechanisms (e.g. slippage, interfacial transport, non-viscous effects, memory effects, and intermittent Brownian motion i.e. stop-and-go diffusion processes). While such effects have received significant attention in the field of nanofluidics,[168] they have not been fully consid-

ered in the field of kerogen modeling. Even if the highly disordered nature of these materials makes the investigation of these mechanisms complex, they are expected to also apply upon gas adsorption and transport. Beyond adsorption/transport coupling within the porosity of kerogens, the thermodynamics of gas is also expected to apply at the interface of kerogen and its external environment. As an important illustration, as already mentioned in this review, the wetting properties of kerogen interfaces was shown to drastically impact hydrocarbon extraction with potential activated transport phenomena in the presence of water.[109] Expected multiphysics effects also include rich phenomena which arise from chemo-mechanical coupling as the adsorption or transport confined fluids is known to be affected by the mechanical response of the kerogen matrix to strains and stresses. Like for other multiphysics aspects, the interplay between mechanical deformation and fluid adsorption has been already identified as a mechanism leading to complex transport in confinement. This includes highly selective ion transport in biomembranes through mechanical solicitation/deformation.[169–171] Moreover, methane, alone or with carbon dioxide, has been the focus of recent studies, but considering heavier hydrocarbons will also help to be closer to geological conditions. From a general viewpoint, investigating the multiphysics phenomena that can occur within kerogen requires very robust and versatile molecular models. While some of the models described in this review provide a very strong basis to tackle such questions, further work is needed to probe their ability to capture these effects in a realistic fashion.

Only a few studies have tried to include the impact of the kerogen mesoporosity on the transport properties while focusing on methane and either neglecting the collective effects or dealing with arbitrarily connected mesopores. Building multiscale strategies accounting for diffusion adsorption in the microporous phase, the impact of the mineral phase, and the permeability of the interface between the microporosity and the mesopores will be a significant challenge in the future. In particular, the multiphysics aspects mentioned above should be integrated with the multiphase nature of shales for more realistic geological conditions. For instance, the thermodynamics and transport properties of fluids adsorbed in

the OM depend on the distribution of stress within the system which, in turn, is determined by the local mechanical properties of the kerogen matrix and the mesopores geometry. In this case, the computational cost of MD simulations will become too important for realistic mesostructures at larger scales. For instance, multi-scales strategies based on pore network modeling, lattice-Boltzmann discretization techniques or random walks simulations – that are commonly used in the field of homogenization in porous media[30–32,162] – could be used.

Biographies

Amaël Obliger got a PhD in theoretical and computational physics from the University Pierre et Marie Curie (Paris, 2014). He was a post-doctoral researcher in 2014-2018 at the Massachusetts Institute of Technology and at the University of California, Berkeley. Then, after being appointed as a junior chair assistant professor at the University of Pau and Pays de l'Adour (France), he joined the University of Bordeaux (France) as a CNRS research officer. His research mostly focus on coupled flow phenomena in complex multi-scales porous media such as electrokinetic couplings in clayey materials in the context of radioactive waste management or transport in source rocks' OM for enhanced oil and gas recovery or carbon sequestration.

Colin Bousige received his PhD in Physics on the study of the structure and dynamics of carbon nanopeapods (University Paris XI and Institute Laue Langevin, Grenoble, 2012). As a post-doctoral researcher at the Massachusetts Institute of Technology, his work then focused on the development of atomistic models of kerogen based on experimental constraints. After a second post-doctoral stay at the Institute of Light and Matter (Lyon, France), he was appointed CNRS researcher in 2017 at the Laboratory of Multimaterials and Interfaces in Lyon, France. His research now focuses on the study of low-dimensional nanomaterials (nanotubes, graphene and related materials) as well as simulations of adsorption and transport in microporous amorphous materials.

Benoit Coasne obtained his PhD in Physics on capillary condensation in nanoporous materials (Paris, 2003). Then, he worked from 2003 to 2005 as a postdoc with Prof. Keith Gubbins on freezing of nanoconfined systems (Raleigh, NC, USA). Benoit Coasne was then appointed CNRS researcher in Montpellier (2005) and promoted CNRS Research Director (2015). From 2012 to 2015, he was leading fundamental research on multiscale modeling of adsorption and transport in the CNRS/MIT lab at MIT in Boston. He is currently affiliated CNRS Research Director in the Interdisciplinary Physics Lab in Grenoble, France. He is also currently appointed Attaché aux Sciences for Veolia Water Technologies. Benoit Coasne was Cofounder and first President of the French Adsorption Society.

Jean-Marc Leyssale received his PhD in theoretical and computational chemistry (Nancy, France, 2003) during which he investigated crystal nucleation in simple molecular fluids. After post-doctoral stays at the National Technical University of Athens (Greece, 2005) and Strahclyde University in Glasgow (Scotland, 2006), studying fluid adsorption and transport in zeolites and developing molecular simulation techniques for the prediction of free energies in crystalline solids, he got appointed as a CNRS research scientist in 2007. His work at the center for ThermoStructural Composites (Univ. Bordeaux) focused on synthetic carbon materials with aerospace and nuclear applications. He got involved with kerogen modeling during a two years stay at the CNRS/MIT joint lab on "MultiScale Materials Science for Energy and the Environment". He's currently back at the University of Bordeaux, pursuing his research at the Institute of Molecular Sciences.

References

(1) Crum-Brown, A. *Geol. Surv. Mem. (Scotl.)*; H.M. Stationery Office, London, 1927.

(2) Cane, R. F. Geological semantics. *Nature* **1970**, *228*, 1009.

(3) Vandenbroucke, M.; Largeau, C. Kerogen origin, evolution and structure. *Org. Geochem.* **2007**, *38*, 719–833.

(4) Hunt, J. M. Distribution of carbon in crust of Earth. *Am. Ass. Petr. Geol. Bull.* **1972**, *56*, 2273–2277.

(5) Durand, B. *Kerogen, Insoluble Organic Matter from Sedimentary Rocks*; Editions Technip: Paris, 1980.

(6) Forsman, J.; Hunt, J. Insoluble organic matter (kerogen) in sedimentary rocks. *Geochim. Cosmochim. Acta* **1958**, *15*, 170–182.

(7) Van Krevelen, D. W. *Coal 3rd edition: Typology - Physics - Chemistry - Constitution*; Elsevier, 1993.

(8) Behar, F.; Vandenbroucke, M. Chemical modeling of kerogen. *Org Geochem.* **1987**, *11*, 15–24.

(9) Rullkötter, J.; Michaelis, W. The structure of kerogen and related materials. A review of recent progress and future trends. *Org. Geochem.* **1990**, *16*, 829–852.

(10) Vandenbroucke, M. Kerogen: from types to models of chemical structure. *Oil Gas Sci. Technol.* **2003**, *58*, 243–269.

(11) Kerr, R. A. Natural Gas From Shale Bursts Onto the Scene. *Science* **2010**, *328*, 1624–1626.

(12) Sovacool, B. K. Cornucopia or curse? Reviewing the costs and benefits of shale gas hydraulic fracturing (fracking). *Renew. Sustain. Energy Rev.* **2014**, *37*, 249–264.

(13) Yuan, J.; Luo, D.; Feng, L. A review of the technical and economic evaluation techniques for shale gas development. *Appl. Energy* **2015**, *148*, 49–65.

(14) Ungerer, P.; Collell, J.; Yiannourakou, M. Molecular modeling of the volumetric and thermodynamic properties of kerogen: Influence of organic type and maturity. *Energy Fuels* **2015**, *29*, 91–105.

(15) Bousige, C.; Ghimbeu, C. M.; Vix-Guterl, C.; Pomerantz, A. E.; Suleimenova, A.; Vaughan, G.; Garbarino, G.; Feygenson, M.; Wildgruber, C.; Ulm, F.-J.; Pellenq, R. J.-M.; Coasne, B. Realistic molecular model of kerogen's nanostructure. *Nat. Mater.* **2016**, *15*, 576–582.

(16) Atmani, L.; Valdenaire, P.-L.; Pellenq, R. J.-M.; Bichara, C.; Damme, H. V.; van Duin, A. C. T.; Ulm, F. J.; Leyssale, J.-M. Simulating the geological fate of terrestrial organic matter: Lignin vs cellulose. *Energy Fuels* **2020**, *34*, 1537–1547.

(17) Leyssale, J.-M.; Valdenaire, P.-L.; Potier, K.; Pellenq, R. J.-M. Replica Exchange Molecular Dynamics Simulation of Organic Matter Evolution: From Lignin to Overmature Type III Kerogen. *Energy Fuels* **2022**, *36*, 14723–14733.

(18) Kelemen, S. R.; Afeworki, M.; Gorbaty, M. L.; Sansone, M.; Kwiatek, P. J.; Walters, C. C.; Freund, H.; Siskin, M.; Bence, A. E.; Curry, D. J.; Solum, M.; Pugmire, R. J.; Vandenbroucke, M.; Leblond, M.; Behar, F. Direct characterization of kerogen by X-ray and solid-state 13C nuclear magnetic resonance methods. *Energy Fuels* **2007**, *21*, 1548–1561.

(19) Hackley, P. C.; Cardott, B. J. Application of Organic Petrography in North American Shale Petroleum Systems: A Review. *Int. J. Coal Geol.* **2016**, *163*, 8–51.

(20) Tissot, B. P.; Welte, D. H. *Petroleum Formation and Occurrence, 2nd edition*; Springer-Verlag, Berlin, 1984.

(21) Suleimenova, A.; Bake, K. D.; Ozkan, A.; Valenza, J. J.; Kleinberg, R. L.; Burnham, A. K.; Ferralis, N.; Pomerantz, A. E. Acid demineralization with critical point drying: A method for kerogen isolation that preserves microstructure. *Fuel* **2014**, *135*, 492–497.

(22) Mathews, J. P.; Chaffee, A. L. The molecular representations of coal - A review. *Fuel* **2012**, *96*, 1–14.

(23) Mathews, J. P.; van Duin, A. C.; Chaffee, A. L. The utility of coal molecular models. *Fuel Process. Technol.* **2011**, *92*, 718–728.

(24) Opletal, G.; Petersen, T.; O'Malley, B.; Snook, I.; McCulloch, D. G.; Marks, N. A.; Yarovsky, I. Hybrid approach for generating realistic amorphous carbon structure using metropolis and reverse Monte Carlo. *Mol. Simul.* **2002**, *28*, 927–938.

(25) Pikunic, J.; Clinard, C.; Cohaut, N.; Gubbins, K. E.; Guet, J.-M.; Pellenq, R. J.-M.; Rannou, I.; Rouzaud, J.-N. Structural modeling of porous carbons: Constrained reverse monte carlo method. *Langmuir* **2003**, *19*, 8565–8582.

(26) Palmer, J.; Brennan, J.; Hurley, M.; Balboa, A.; Gubbins, K. Detailed structural models for activated carbons from molecular simulation. *Carbon* **2009**, *47*, 2904–2913.

(27) Striolo, A.; Cole, D. R. Understanding Shale Gas: Recent Progress and Remaining Challenges. *Energy Fuels* **2017**, *31*, 10300–10310.

(28) Firouzi, M.; Wilcox, J. Molecular modeling of carbon dioxide transport and storage in porous carbon-based materials. *Microporous and Mesoporous Materials* **2012**, *158*, 195–203.

(29) Chen, L.; Kang, Q.; Dai, Z.; Viswanathan, H. S.; Tao, W. Permeability prediction of shale matrix reconstructed using the elementary building block model. *Fuel* **2015**, *160*, 346–356.

(30) Chen, L.; Zhang, L.; Kang, Q.; Viswanathan, H. S.; Yao, J.; Tao, W. Nanoscale simulation of shale transport properties using the lattice Boltzmann method: permeability and diffusivity. *Scientific Reports* **2015**, *5*.

(31) Wang, J.; Chen, L.; Kang, Q.; Rahman, S. S. Apparent permeability prediction of organic shale with generalized lattice Boltzmann model considering surface diffusion effect. *Fuel* **2016**, *181*, 478–490.

(32) Mehmani, A.; Prodanović, M.; Javadpour, F. Multiscale, Multiphysics Network Modeling of Shale Matrix Gas Flows. *Transport in Porous Media* **2013**, *99*, 377–390.

(33) Clarkson, C. R.; Nobakht, M.; Kaviani, D.; Ertekin, T. Production analysis of tight-gas and shale-gas reservoirs using the dynamic-slippage concept. *SPE Journal* **2012**, *17*, 230–242.

(34) Sinha, S.; Braun, E. M.; Determan, M. D.; Passey, Q. R.; Leonardi, S. A.; Boros, J. A.; Wood, A. C.; Zirkle, T.; Kudva, R. A. Steady-State Permeability Measurements on Intact Shale Samples at Reservoir Conditions - Effect of Stress, Temperature, Pressure, and Type of Gas. 2013; https://doi.org/10.2118/164263-MS, SPE-164263-MS.

(35) Aguilera, R. Flow units: From conventional to tight-gas to shale-gas to tight-oil to shale-oil reservoirs. *SPE Reservoir Evaluation and Engineering* **2014**, *17*, 190–208.

(36) Zhang, H.; Ahmed, M.; Zhan, J.-H. Recent advances in molecular simulation of oil shale kerogen. *Fuel* **2022**, *316*, 123392.

(37) Zhao, Y.; Li, W.; Zhan, S.; Jin, Z. Breakthrough pressure of oil displacement by water through the ultra-narrow kerogen pore throat from the Young–Laplace equation and molecular dynamic simulations. *Phys. Chem. Chem. Phys.* **2022**,

(38) Alafnan, S. The self-diffusivity of natural gas in the organic nanopores of source rocks. *Phys. Fluids* **2022**, *34*, 042004.

(39) Tesson, S.; Firoozabadi, A. Methane adsorption and self-diffusion in shale kerogen and slit nanopores by molecular simulations. *J. Phys. Chem. C* **2018**, *122*, 23528–23542.

(40) Kang, D.; Zhao, Y.-P. Predicting the molecular models, types, and maturity of kerogen in shale using machine learning and multi-NMR spectra. *Energy Fuels* **2022**, *36*, 5749–5761.

(41) Huang, M.; Xu, H.; Yu, H.; Zhang, H.; Micheal, M.; Yuan, X.; Wu, H. Fast prediction of methane adsorption in shale nanopores using kinetic theory and machine learning algorithm. *Chem. Eng. J.* **2022**, *446*, 137221.

(42) Oberlin, A.; Villey, M.; Combaz, A. Influence of elemental composition on carbonization: Pyrolysis of kerosene shale and kuckersite. *Carbon* **1980**, *18*, 347–353.

(43) Siskin, M.; Scouten, C.; Rose, K.; Aczel, T.; Colgrove, S.; Pabst, R. *Composition, geochemistry and conversion of oil shales*; Springer, 1995; pp 143–158.

(44) Lille, U.; Heinmaa, I.; Pehk, T. Molecular model of Estonian kukersite kerogen evaluated by 13C MAS NMR spectra. *Fuel* **2003**, *82*, 799–804.

(45) Faulon, J.; Vandenbroucke, M.; Drappier, J.; Behar, F.; Romero, M. 3D chemical model for geological macromolecules. *Org. Geochem.* **1990**, *16*, 981–993.

(46) Zhang, L.; LeBoeuf, E. J. A molecular dynamics study of natural organic matter: 1. Lignin, kerogen and soot. *Org. Geochem.* **2009**, *40*, 1132–1142.

(47) Orendt, A. M.; Pimienta, I. S.; Badu, S. R.; Solum, M. S.; Pugmire, R. J.; Facelli, J. C.; Locke, D. R.; Chapman, K. W.; Chupas, P. J.; Winans, R. E. Three-dimensional structure of the siskin green river oil shale kerogen model: A comparison between calculated and observed properties. *Energy Fuels* **2013**, *27*, 702–710.

(48) Ru, X.; Cheng, Z.; Song, L.; Wang, H.; Li, J. Experimental and computational studies on the average molecular structure of Chinese Huadian oil shale kerogen. *J. Mol. Struct.* **2012**, *1030*, 10–18.

(49) Vasileiadis, M.; Peristeras, L. D.; Papavasileiou, K. D.; Economou, I. G. Modeling of bulk kerogen porosity: Methods for control and characterization. *Energy Fuels* **2017**, *31*, 6004–6018.

(50) Michalec, L.; Lísal, M. Molecular simulation of shale gas adsorption onto overmature type II model kerogen with control microporosity. *Mol. Phys.* **2016**, *115*, 1086–1103.

(51) Collell, J.; Ungerer, P.; Galliero, G.; Yiannourakou, M.; Montel, F.; Pujol, M. Molecular simulation of bulk organic matter in type II shales in the middle of the oil formation window. *Energy Fuels* **2014**, *28*, 7457–7466.

(52) Li, Z.; Yao, J.; Firoozabadi, A. Kerogen Swelling in Light Hydrocarbon Gases and Liquids and Validity of Schroeder's Paradox. *J. Phys. Chem. C* **2021**, *125*, 8137–8147.

(53) Huang, L.; Ning, Z.; Wang, Q.; Qi, R.; Li, J.; Zeng, Y.; Ye, H.; Qin, H. Thermodynamic and structural characterization of bulk organic matter in Chinese Silurian shale: experimental and molecular modeling studies. *Energy Fuels* **2017**, *31*, 4851–4865.

(54) Guan, X.-H.; Liu, Y.; Wang, D.; Wang, Q.; Chi, M.-S.; Liu, S.; Liu, C.-G. Three-dimensional structure of a Huadian oil shale kerogen model: An experimental and theoretical study. *Energy Fuels* **2015**, *29*, 4122–4136.

(55) Pan, S.; Zhou, H.; Wang, Q.; Bai, J.; Cui, D.; Wang, X. Experimental and molecular simulation studies of Huadian oil shale kerogen. *ACS Omega* **2022**, *7*, 17253–17269.

(56) Pan, S.; Wang, Q.; Bai, J.; Chi, M.; Cui, D.; Wang, Z.; Liu, Q.; Xu, F. Molecular structure and electronic properties of oil shale kerogen: An experimental and molecular modeling study. *Energy Fuels* **2018**, *32*, 12394–12404.

(57) Liu, Y.; Liu, S.; Zhang, R.; Zhang, Y. The molecular model of Marcellus shale kerogen: Experimental characterization and structure reconstruction. *Int. J. Coal Geol.* **2021**, *246*, 103833.

(58) Zhang, C.; Yao, Y.; Elsworth, D.; Liu, D.; Ju, Y.; Dong, Y.; Ye, S. Microstructure

characterization of kerogen in mature shale: Molecular investigation of micropore development. *J. Nat. Gas Sci. Eng.* **2021**, *95*, 104239.

(59) Wang, X.; Zhu, Y.; Chen, S.; Dai, X.; Xu, Q.; Song, Y.; Mathews, J. P. Molecular structure evaluation and image-guided atomistic representation of marine kerogen from longmaxi shale. *Energy Fuels* **2021**, *35*, 7981–7992.

(60) Palmer, J.; Llobet, A.; Yeon, S.-H.; Fischer, J.; Shi, Y.; Gogotsi, Y.; Gubbins, K. Modeling the structural evolution of carbide-derived carbons using quenched molecular dynamics. *Carbon* **2010**, *48*, 1116–1123.

(61) Obliger, A.; Valdenaire, P.-L.; Capit, N.; Ulm, F. J.; Pellenq, R. J.-M.; Leyssale, J.-M. Poroelasticity of methane-loaded mature and immature kerogen from molecular simulations. *Langmuir* **2018**, *34*, 13766–13780.

(62) McGreevy, R. L.; Pusztai, L. Reverse Monte Carlo simulation: A new technique for the determination of disordered structures. *Mol. Simul.* **1988**, *1*, 359–367.

(63) McGreevy, R. RMC: progress, problems and prospects. *Nucl. Instrum. Methods Phys. Res. A* **1995**, *354*, 1–16.

(64) Keen, D. A. Refining disordered structural models using reverse Monte Carlo methods: Application to vitreous silica. *Phase Transit.* **1997**, *61*, 109–124.

(65) Biswas, P.; Atta-Fynn, R.; Drabold, D. A. Reverse Monte Carlo modeling of amorphous silicon. *Phys. Rev. B* **2004**, *69*.

(66) Pikunic, J.; Llewellyn, P.; Pellenq, R.; Gubbins, K. E. Argon and nitrogen adsorption in disordered nanoporous carbons: Simulation and experiment. *Langmuir* **2005**, *21*, 4431–4440.

(67) Gereben, O.; Pusztai, L. RMC_POT: A computer code for reverse Monte Carlo modeling the structure of disordered systems containing molecules of arbitrary complexity. *J. Comput. Chem.* **2012**, *33*, 2285–2291.

(68) Jain, S. K.; Pellenq, R. J.-M.; Pikunic, J. P.; Gubbins, K. E. Molecular modeling of porous carbons using the hybrid reverse Monte Carlo method. *Langmuir* **2006**, *22*, 9942–9948.

(69) Nguyen, T. X.; Bhatia, S. K.; Jain, S. K.; Gubbins, K. E. Structure of saccharose-based carbon and transport of confined fluids: hybrid reverse Monte Carlo reconstruction and simulation studies. *Mol. Simul.* **2006**, *32*, 567–577.

(70) Bousige, C.; Boţan, A.; Ulm, F.-J.; Pellenq, R. J.-M.; Coasne, B. Optimized molecular reconstruction procedure combining hybrid reverse Monte Carlo and molecular dynamics. *J. Chem. Phys.* **2015**, *142*, 114112.

(71) Hantal, G.; Brochard, L.; Cordeiro, M. N. D. S.; Ulm, F. J.; Pellenq, R. J.-M. Surface chemistry and atomic-scale reconstruction of Kerogen–Silica composites. *J. Phys. Chem. C* **2014**, *118*, 2429–2438.

(72) Van Duin, A. C.; Dasgupta, S.; Lorant, F.; Goddard, W. A. ReaxFF: a reactive force field for hydrocarbons. *J. Phys. Chem. A* **2001**, *105*, 9396–9409.

(73) Salmon, E.; van Duin, A. C.; Lorant, F.; Marquaire, P.-M.; Goddard III, W. A. Early maturation processes in coal. Part 2: Reactive dynamics simulations using the ReaxFF reactive force field on Morwell Brown coal structures. *Org. Geochem.* **2009**, *40*, 1195–1209.

(74) Liu, X.; Zhan, J.-H.; Lai, D.; Liu, X.; Zhang, Z.; Xu, G. Initial pyrolysis mechanism of oil shale kerogen with reactive molecular dynamics simulation. *Energy Fuels* **2015**, *29*, 2987–2997.

(75) Qian, Y.; Zhan, J.-H.; Lai, D.; Li, M.; Liu, X.; Xu, G. Primary understanding of non-isothermal pyrolysis behavior for oil shale kerogen using reactive molecular dynamics simulation. *Int. J. Hydrog. Energy* **2016**, *41*, 12093–12100.

(76) Pawar, G.; Meakin, P.; Huang, H. Reactive molecular dynamics simulation of kerogen thermal maturation and cross-linking pathways. *Energy Fuels* **2017**, *31*, 11601–11614.

(77) Zheng, M.; Wang, Z.; Li, X.; Qiao, X.; Song, W.; Guo, L. Initial reaction mechanisms of cellulose pyrolysis revealed by ReaxFF molecular dynamics. *Fuel* **2016**, *177*, 130–141.

(78) Zhang, T.; Li, X.; Qiao, X.; Zheng, M.; Guo, L.; Song, W.; Lin, W. Initial mechanisms for an overall behavior of lignin pyrolysis through large-scale ReaxFF molecular dynamics simulations. *Energy Fuels* **2016**, *30*, 3140–3150.

(79) Atmani, L.; Bichara, C.; Pellenq, R. J.-M.; Damme, H. V.; van Duin, A. C. T.; Raza, Z.; Truflandier, L. A.; Obliger, A.; Kralert, P. G.; Ulm, F. J.; Leyssale, J.-M. From cellulose to kerogen: molecular simulation of a geological process. *Chem. Sci.* **2017**, *8*, 8325–8335.

(80) Sugita, Y.; Okamoto, Y. Replica-exchange molecular dynamics method for protein folding. *Chem. Phys. Lett.* **1999**, *314*, 141–151.

(81) Pitera, J. W.; Swope, W. Understanding folding and design: Replica-exchange simulations of"Trp-cage"miniproteins. *Proc. Natl. Acad. Sci.* **2003**, *100*, 7587–7592.

(82) Earl, D. J.; Deem, M. W. Parallel tempering: Theory, applications, and new perspectives. *Phys. Chem. Chem. Phys.* **2005**, *7*, 3910–3916.

(83) Farbos, B.; Weisbecker, P.; Fischer, H.; Da Costa, J.-P.; Lalanne, M.; Chollon, G.; Germain, C.; Vignoles, G.; Leyssale, J.-M. Nanoscale structure and texture of highly

anisotropic pyrocarbons revisited with transmission electron microscopy, image processing, neutron diffraction and atomistic modeling. *Carbon* **2014**, *80*, 472–489.

(84) de Tomas, C.; Aghajamali, A.; Jones, J. L.; Lim, D. J.; López, M. J.; Suarez-Martinez, I.; Marks, N. A. Transferability in interatomic potentials for carbon. *Carbon* **2019**, *155*, 624–634.

(85) Toh, C.-T.; Zhang, H.; Lin, J.; Mayorov, A. S.; Wang, Y.-P.; Orofeo, C. M.; Ferry, D. B.; Andersen, H.; Kakenov, N.; Guo, Z.; Abidi, I. H.; Sims, H.; Suenaga, K.; Pantelides, S. T.; Özyilmaz, B. Synthesis and properties of free-standing monolayer amorphous carbon. *Nature* **2020**, *577*, 199–203.

(86) Singh, M.; Vander Wal, R. L. Nanostructure quantification of carbon blacks. *C* **2019**, *5*, 2.

(87) Sharma, A.; Kyotani, T.; Tomita, A. Comparison of structural parameters of PF carbon from XRD and HRTEM techniques. *Carbon* **2000**, *38*, 1977–1984.

(88) Clarkson, C. R.; Freeman, M.; He, L.; Agamalian, M.; Melnichenko, Y.; Mastalerz, M.; Bustin, R. M.; Radliński, A.; Blach, T. Characterization of tight gas reservoir pore structure using USANS/SANS and gas adsorption analysis. *Fuel* **2012**, *95*, 371–385.

(89) Clarkson, C. R.; Solano, N.; Bustin, R. M.; Bustin, A.; Chalmers, G. R.; He, L.; Melnichenko, Y. B.; Radliński, A.; Blach, T. P. Pore structure characterization of North American shale gas reservoirs using USANS/SANS, gas adsorption, and mercury intrusion. *Fuel* **2013**, *103*, 606–616.

(90) Chiang, W.-S.; Chen, J.-H.; Jacobi, D.; Yildirim, T.; Turkoglu, D.; Althaus, S.; Liu, Y. Structural properties of kerogens with different maturities. *Energy Fuels* **2020**, *34*, 12354–12365.

(91) Thomas, J. J.; Valenza II, J. J.; Craddock, P. R.; Bake, K. D.; Pomerantz, A. E. The neutron scattering length density of kerogen and coal as determined by CH3OH/CD3OH exchange. *Fuel* **2014**, *117*, 801–808.

(92) Wu, H.; Wen, L.; Zhang, L.; Wang, D.; Li, N.; Yang, M. Gas adsorption capacity of type-II kerogen at a varying burial depth. *Energy Fuels* **2022**, *36*, 7472–7482.

(93) Wang, J.; Liu, Y.; Yang, C.; Jiang, W.; Li, Y.; Xiong, Y., et al. Evolution of mechanical properties of kerogen with thermal maturity. *Mar. Pet. Geol.* **2022**, *145*, 105906.

(94) Kashinath, A.; Szulczewski, M. L.; Dogru, A. H. Modeling the effect of maturity on the elastic moduli of kerogen using atomistic simulations. *Energy Fuels* **2020**, *34*, 1378–1385.

(95) Wu, T.; Firoozabadi, A. Fracture toughness and surface energy density of kerogen by molecular dynamics simulations in tensile failure. *J. Phys. Chem. C* **2020**, *124*, 15895–15901.

(96) Wu, T.; Firoozabadi, A. Mechanical properties and failure envelope of kerogen matrix by molecular dynamics simulations. *J. Phys. Chem. C* **2020**, *124*, 2289–2294.

(97) Afagwu, C.; Al-Afnan, S.; Patil, S.; Aljaberi, J.; Mahmoud, M. A.; Li, J. The impact of pore structure and adsorption behavior on kerogen tortuosity. *Fuel* **2021**, *303*, 121261.

(98) Alafnan, S.; Solling, T.; Mahmoud, M. Effect of kerogen thermal maturity on methane adsorption capacity: A molecular modeling approach. *Molecules* **2020**, *25*, 3764.

(99) Alafnan, S. Petrophysics of kerogens based on realistic structures. *ACS Omega* **2021**, *6*, 9549–9558.

(100) He, S.; Jiang, Y.; Conrad, J. C.; Qin, G. Molecular simulation of natural gas transport and storage in shale rocks with heterogeneous nano-pore structures. *J. Pet. Sci. Eng.* **2015**, *133*, 401–409.

(101) Collell, J.; Galliero, G.; Gouth, F.; Montel, F.; Pujol, M.; Ungerer, P.; Yiannourakou, M. Molecular simulation and modelisation of methane/ethane mixtures adsorption onto a microporous molecular model of kerogen under typical reservoir conditions. *Microporous Mesoporous Mater.* **2014**, *197*, 194–203.

(102) Falk, K.; Pellenq, R.; Ulm, F. J.; Coasne, B. Effect of chain length and pore accessibility on alkane adsorption in kerogen. *Energy Fuels* **2015**, *29*, 7889–7896.

(103) Wang, R.; Li, J.; Gibelli, L.; Guo, Z.; Borg, M. K. Sub-nanometre pore adsorption of methane in kerogen. *Chem. Eng. J.* **2021**, *426*, 130984.

(104) Huang, L.; Ning, Z.; Wang, Q.; Ye, H.; Wang, Z.; Sun, Z.; Qin, H. Microstructure and adsorption properties of organic matter in Chinese Cambrian gas shale: Experimental characterization, molecular modeling and molecular simulation. *Int. J. Coal Geol.* **2018**, *198*, 14–28.

(105) Wu, T.; Zhao, H.; Tesson, S.; Firoozabadi, A. Absolute adsorption of light hydrocarbons and carbon dioxide in shale rock and isolated kerogen. *Fuel* **2019**, *235*, 855–867.

(106) Zhang, J.; Han, D.; Wang, C.; Lin, W.; Zhang, H.; Li, S. Molecular simulation of shale gas adsorption in type III kerogen organic matter. *Pet. Sci. Technol.* **2022**, *40*, 1–11.

(107) Myers, A. L.; Prausnitz, J. M. Thermodynamics of mixed-gas adsorption. *AIChE J.* **1965**, *11*, 121–127.

(108) Glatz, G.; Alafnan, S.; Raza, A.; Mahmoud, M. Multicomponent gas adsorption behavior of kerogen: A molecular investigation. *Energy Fuels* **2022**, *36*, 6695–6710.

(109) Lee, T.; Bocquet, L.; Coasne, B. Activated desorption at heterogeneous interfaces and long-time kinetics of hydrocarbon recovery from nanoporous media. *Nat. Commun.* **2016**, *7*, 11890.

(110) Zhang, Z.; Liu, H.; Wang, J. Energetics of interfacial interactions of hydrocarbon fluids with kerogen and calcite using molecular modeling. *Energy Fuels* **2020**, *34*, 4251–4259.

(111) Zhao, T.; Li, X.; Zhao, H.; Li, M. Molecular simulation of adsorption and thermodynamic properties on type II kerogen: Influence of maturity and moisture content. *Fuel* **2017**, *190*, 198–207.

(112) Ren, W.; Guo, J.; Zeng, F.; Wang, T. Modeling of high-pressure methane adsorption on wet shales. *Energy Fuels* **2019**, *33*, 7043–7051.

(113) Zhao, T.; Li, X.; Ning, Z.; Zhao, H.; Li, M. Molecular simulation of methane adsorption on type II kerogen with the impact of water content. *J. Pet. Sci. Eng.* **2018**, *161*, 302–310.

(114) Billemont, P.; Coasne, B.; Weireld, G. D. Adsorption of carbon dioxide, methane, and their mixtures in porous carbons: Effect of surface chemistry, water content, and pore disorder. *Langmuir* **2013**, *29*, 3328–3338.

(115) Chong, L.; Sanguinito, S.; Goodman, A. L.; Myshakin, E. M. Molecular characterization of carbon dioxide, methane, and water adsorption in micropore space of kerogen matrix. *Fuel* **2021**, *283*, 119254.

(116) Huang, L.; Ning, Z.; Wang, Q.; Qi, R.; Zeng, Y.; Qin, H.; Ye, H.; Zhang, W. Molecular simulation of adsorption behaviors of methane, carbon dioxide and their mixtures on kerogen: Effect of kerogen maturity and moisture content. *Fuel* **2018**, *211*, 159–172.

(117) Li, J.; Wang, Y.; Chen, Z.; Rahman, S. S. Insights into the molecular competitive adsorption mechanism of CH4/CO2 in a kerogen matrix in the presence of moisture, salinity, and ethane. *Langmuir* **2021**, *37*, 12732–12745.

(118) Huang, L.; Ning, Z.; Wang, Q.; Zhang, W.; Cheng, Z.; Wu, X.; Qin, H. Effect of organic

type and moisture on CO2/CH4 competitive adsorption in kerogen with implications for CO2 sequestration and enhanced CH4 recovery. *Appl. Energy* **2018**, *210*, 28–43.

(119) Omari, A.; Wang, C.; Li, Y.; Xu, X. The progress of enhanced gas recovery (EGR) in shale gas reservoirs: A review of theory, experiments, and simulations. *J. Pet. Sci. Eng.* **2022**, *213*, 110461.

(120) Wang, Z.; Li, Y.; Liu, H.; Zeng, F.; Guo, P.; Jiang, W. Study on the adsorption, diffusion and permeation selectivity of shale gas in organics. *Energies* **2017**, *10*, 142.

(121) Pathak, M.; Huang, H.; Meakin, P.; Deo, M. Molecular investigation of the interactions of carbon dioxide and methane with kerogen: Application in enhanced shale gas recovery. *J. Nat. Gas Sci. Eng.* **2018**, *51*, 1–8.

(122) Wang, T.; Tian, S.; Li, G.; Sheng, M. Selective adsorption of supercritical carbon dioxide and methane binary mixture in shale kerogen nanopores. *J. Nat. Gas Sci. Eng.* **2018**, *50*, 181–188.

(123) Wang, T.; Tian, S.; Li, G.; Sheng, M.; Ren, W.; Liu, Q.; Zhang, S. Molecular simulation of CO2/CH4 competitive adsorption on shale kerogen for CO2 sequestration and enhanced gas recovery. *J. Phys. Chem. C* **2018**, *122*, 17009–17018.

(124) Alafnan, S.; Falola, Y.; Mansour, O. A.; Al Samadony, K.; Awotunde, A.; Aljawad, M. Enhanced recovery from organic-rich shales through carbon dioxide injection: Molecular-level investigation. *Energy Fuels* **2020**, *34*, 16089–16098.

(125) Li, Y.; Lu, L.; Zhu, J.; Yang, Z.; Qu, J.; Xue, H.; Ouyang, J. Molecular simulation of CH4 nanoscale behavior and enhanced gas recovery in organic-rich shale. *Geofluids* **2022**, *2022*, 2420869.

(126) Zeng, K.; Jiang, P.; Lun, Z.; Xu, R. Molecular simulation of carbon dioxide and methane adsorption in shale organic nanopores. *Energy Fuels* **2018**, *33*, 1785–1796.

(127) Xu, H.; Yu, H.; Fan, J.; Xia, J.; Wang, F.; Wu, H. Enhanced gas recovery in kerogen pyrolytic pore network: Molecular simulations and theoretical analysis. *Energy Fuels* **2021**, *35*, 2253–2267.

(128) Wang, S.; Yao, X.; Feng, Q.; Javadpour, F.; Yang, Y.; Xue, Q.; Li, X. Molecular insights into carbon dioxide enhanced multi-component shale gas recovery and its sequestration in realistic kerogen. *Chem. Eng. J.* **2021**, *425*, 130292.

(129) Tesson, S.; Firoozabadi, A. Deformation and swelling of kerogen matrix in light hydrocarbons and carbon dioxide. *J. Phys. Chem. C* **2019**, *123*, 29173–29183.

(130) Wu, J.; Huang, P.; Maggi, F.; Shen, L. Effect of sorption-induced deformation on methane flow in kerogen slit pores. *Fuel* **2022**, *325*, 124886.

(131) Babatunde, K. A.; Negash, B. M.; Mojid, M. R.; Ahmed, T. Y.; Jufar, S. R. Molecular simulation study of CO2/CH4 adsorption on realistic heterogeneous shale surfaces. *Appl. Surf. Sci.* **2021**, *543*, 148789.

(132) Larsen, J. W.; Li, S. Solvent swelling studies of Green River kerogen. *Energy Fuels* **1994**, *8*, 932–936.

(133) Pathak, M.; Kweon, H.; Deo, M.; Huang, H. Kerogen swelling and confinement: Its implication on fluid thermodynamic properties in shales. *Sci. Rep.* **2017**, *7*, 12530.

(134) Ertas, D.; Kelemen, S. R.; Halsey, T. C. Petroleum expulsion part 1. Theory of kerogen swelling in multicomponent solvents. *Energy Fuels* **2006**, *20*, 295–300.

(135) Coussy, O. *Mechanics and Physics of Porous Solids*; John Wiley & Sons, Ltd, 2010.

(136) Brochard, L.; Vandamme, M.; Pellenq, R.-M. Poromechanics of microporous media. *J. Mech. Phys. Solids* **2012**, *60*, 606–622.

(137) Huang, L.; Ning, Z.; Wang, Q.; Qi, R.; Cheng, Z.; Wu, X.; Zhang, W.; Qin, H. Kerogen deformation upon CO2/CH4 competitive sorption: Implications for CO2 sequestration and enhanced CH4 recovery. *J. Pet. Sci. Eng.* **2019**, *183*, 106460.

(138) Huang, L.; Ning, Z.; Wang, Q.; Qi, R.; Cheng, Z.; Wu, X.; Zhang, W.; Qin, H. Molecular insights into kerogen deformation induced by CO2/CH4 sorption: Effect of maturity and moisture. *Energy Fuels* **2019**, *33*, 4792–4805.

(139) Falk, K.; Coasne, B.; Pellenq, R.; Ulm, F.-J.; Bocquet, L. Subcontinuum mass transport of condensed hydrocarbons in nanoporous media. *Nat. Commun.* **2015**, *6*, 6949.

(140) Coasne, B.; Jain, S. K.; Gubbins, K. E. Adsorption, structure and dynamics of fluids in ordered and disordered models of porous carbons. *Mol. Phys.* **2006**, *104*, 3491–3499.

(141) Coasne, B.; Jain, S. K.; Gubbins, K. E. Adsorption and dynamics of argon in porous carbons. *Eur. Phys. J. Spec. Top.* **2007**, *141*, 121–125.

(142) Boţan, A.; Vermorel, R.; Ulm, F.-J.; Pellenq, R. J.-M. Molecular simulations of supercritical fluid permeation through disordered microporous carbons. *Langmuir* **2013**, *29*, 9985–9990.

(143) Obliger, A.; Pellenq, R.; Ulm, F.-J.; Coasne, B. Free volume theory of hydrocarbon mixture transport in nanoporous materials. *J. Phys. Chem. Lett.* **2016**, *7*, 3712–3717.

(144) Obliger, A.; Ulm, F.-J.; Pellenq, R. Impact of nanoporosity on hydrocarbon transport in shales' organic matter. *Nano Lett.* **2018**, *18*, 832–837.

(145) Collell, J.; Galliero, G.; Vermorel, R.; Ungerer, P.; Yiannourakou, M.; Montel, F.; Pujol, M. Transport of multicomponent hydrocarbon mixtures in shale organic matter by molecular simulations. *J. Phys. Chem. C* **2015**, *119*, 22587–22595.

(146) Ariskina, K.; Galliéro, G.; Obliger, A. Free volume model for transport in flexible kerogen of source rock's organic matter. *J. Phys. Chem. B* **2022**,

(147) Sui, H.; Zhang, F.; Wang, Z.; Wang, D.; Wang, Y. Effect of kerogen maturity, water content for carbon dioxide, methane, and their mixture adsorption and diffusion in kerogen: A computational investigation. *Langmuir* **2020**, *36*, 9756–9769.

(148) Yu, K. B.; Bowers, G. M.; Loganathan, N.; Kalinichev, A. G.; Yazaydin, A. O. Diffusion behavior of methane in 3D kerogen models. *Energy Fuels* **2021**, *35*, 16515–16526.

(149) Vasileiadis, M.; Peristeras, L. D.; Papavasileiou, K. D.; Economou, I. G. Transport properties of shale gas in relation to kerogen porosity. *J. Phys. Chem. C* **2018**, *122*, 6166–6177.

(150) Perez, F.; Devegowda, D. Hydrocarbon self-diffusion and assessing the validity of graham's law under nanoporous confinement in shales. *Energy Fuels* **2021**, *35*, 10512–10518.

(151) Wu, T.; Firoozabadi, A. Effect of microstructural flexibility on methane flow in kerogen matrix by molecular dynamics simulations. *J. Phys. Chem. C* **2019**, *123*, 10874–10880.

(152) Obliger, A.; Valdenaire, P.-L.; Ulm, F.-J.; Pellenq, R. J.-M.; Leyssale, J.-M. Methane diffusion in a flexible kerogen matrix. *J. Phys. Chem. B* **2019**, *123*, 5635–5640.

(153) Zhang, L.; Li, J.; Jia, D.; Zhao, Y.; Xie, C.; Tao, Z. Study on the adsorption phenomenon in shale with the combination of molecular dynamic simulation and fractal analysis. *Fractals* **2018**, *26*, 1840004.

(154) Zhou, B.; Xu, R.; Jiang, P. Novel molecular simulation process design of adsorption in realistic shale kerogen spherical pores. *Fuel* **2016**, *180*, 718–726.

(155) Chang, C.; Zhang, J.; Hu, H.; Zhang, D.; Zhao, Y. Molecular simulation of adsorption in deep marine shale gas reservoirs. *Energies* **2022**, *15*, 944.

(156) Huang, S.; Ma, X.; Yang, H.; Wu, J.; Zhang, J.; Zhao, S.; Zhang, D.; Ren, C.; Huang, L. Experimental characterization and molecular modeling of kerogen in Sil-

urian deep gas shale from southern Sichuan Basin, China. *Energy Rep.* **2022**, *8*, 1497–1507.

(157) Coasne, B.; Galarneau, A.; Gerardin, C.; Fajula, F.; Villemot, F. Molecular simulation of adsorption and transport in hierarchical porous materials. *Langmuir* **2013**, *29*, 7864–7875.

(158) Deliere, L.; Villemot, F.; Farrusseng, D.; Galarneau, A.; Topin, S.; Coasne, B. Adsorption in heterogeneous porous media: Hierarchical and composite solids. *Microporous Mesoporous Mater.* **2016**, *229*, 145–154.

(159) Rezlerová, E.; Brennan, J. K.; Lísal, M. Methane and carbon dioxide in dual-porosity organic matter: Molecular simulations of adsorption and diffusion. *AIChE J.* **2021**, *67*, e16655.

(160) Sholl, D. S. Understanding macroscopic diffusion of adsorbed molecules in crystalline nanoporous materials via atomistic simulations. *Acc. Chem. Res.* **2006**, *39*, 403–411.

(161) Magnin, Y.; Berthonneau, J.; Chanut, N.; Ferry, D.; Grauby, O.; Jorand, R.; Ulm, F. J.; Chaput, E.; Pellenq, R. Hydrocarbon diffusion in mesoporous carbon materials: Implications for unconventional gas recovery. *ACS Appl. Nano Mater.* **2020**, *3*, 7604–7610.

(162) Berthonneau, J.; Obliger, A.; Valdenaire, P.-L.; Grauby, O.; Ferry, D.; Chaudanson, D.; Levitz, P.; Kim, J. J.; Ulm, F.-J.; Pellenq, R. J.-M. Mesoscale structure, mechanics, and transport properties of source rocks' organic pore networks. *Proc. Natl. Acad. Sci.* **2018**, *115*, 12365–12370.

(163) Tóth, G.; Baranyai, A. Molecular dynamics analog of the reverse Monte Carlo method. *J. Chem. Phys.* **2001**, *114*, 2027–2035.

(164) Ishida, M.; Ohba, T. Hybrid reverse molecular dynamics simulation as new approach to determination of carbon nanostructure of carbon blacks. *Sci. Rep.* **2020**, *10*, 3622.

(165) Valdenaire, P.-L.; Pellenq, R. J.; Ulm, F. J.; Van Duin, A. C.; Leyssale, J.-M. Timescale prediction of complex multi-barrier pathways using flux sampling molecular dynamics and 1D kinetic integration: Application to cellulose dehydration. *J. Chem. Phys.* **2020**, *152*, 024123.

(166) Rowe, P.; Deringer, V. L.; Gasparotto, P.; Csányi, G.; Michaelides, A. An accurate and transferable machine learning potential for carbon. *J. Chem. Phys.* **2020**, *153*, 034702.

(167) Hantal, G.; Brochard, L.; Pellenq, R. J.-M.; Ulm, F.-J.; Coasne, B. Role of Interfaces in Elasticity and Failure of Clay–Organic Nanocomposites: Toughening upon Interface Weakening? *Langmuir* **2017**, *33*, 11457–11466.

(168) Bocquet, L.; Charlaix, E. Nanofluidics, from bulk to interfaces. *Chemical Society Reviews* **2010**, *39*, 1073–1095.

(169) Marbach, S.; Bocquet, L. Active sieving across driven nanopores for tunable selectivity. *J. Chem. Phys.* **2017**, *147*, 154701.

(170) Cox, C. D.; Bavi, N.; Martinac, B. Biophysical principles of ion-channel-mediated mechanosensory transduction. *Cell Reports* **2019**, *29*, 1–12.

(171) Marcotte, A.; Mouterde, T.; Niguès, A.; Siria, A.; Bocquet, L. Mechanically activated ionic transport across single-digit carbon nanotubes. *Nature Materials* **2020**, *19*, 1057–1061.

TOC Graphic